AUTOPHAGY
2023, VOL. 19, NO. 9, 2538–2557
https://doi.org/10.1080/15548627.2023.2200625

Taylor & Francis
Taylor & Francis Group

NR3C1/Glucocorticoid receptor activation promotes pancreatic β-cell autophagy overload in response to glucolipotoxicity

Tijun Wu [a], Yixue Shao[a], Xirui Li[a], Tao Wu[a], Ling Yu[a], Jin Liang[a], Yaru Zhang[a], Jiahui Wang[a], Tong Sun[a], Yunxia Zhu[a], Xiaoai Chang[a], Shusen Wang[b], Fang Chen[a], and Xiao Han [a]

[a]Key Laboratory of Human Functional Genomics of Jiangsu Province, Nanjing Medical University, Nanjing, Jiangsu, China; [b]Organ Transplant Center, Tianjin First Central Hospital, Nankai University, Tianjin, China

ABSTRACT

Diabetes is a complex and heterogeneous disorder characterized by chronic hyperglycemia. Its core cause is progressively impaired insulin secretion by pancreatic β-cell failures, usually upon a background of preexisting insulin resistance. Recent studies demonstrate that macroautophagy/autophagy is essential to maintain architecture and function of β-cells, whereas excessive autophagy is also involved in β-cell dysfunction and death. It has been poorly understood whether autophagy plays a protective or harmful role in β-cells, while we report here that it is dependent on NR3C1/glucocorticoid receptor activation. We proved that deleterious hyperactive autophagy happened only upon NR3C1 activation in β-cells under glucolipotoxic conditions, which eventually promoted diabetes. The transcriptome and the *N6*-methyladenosine (m^6A) methylome revealed that NR3C1-enhancement upregulated the RNA demethylase FTO (fat mass and obesity associated) protein in β-cells, which caused diminished m^6A modifications on mRNAs of four core *Atg* (autophagy related) genes (*Atg12, Atg5, Atg16l2, Atg9a*) and, hence, hyperactive autophagy and defective insulin output; by contrast, FTO inhibition, achieved by the specific FTO inhibitor Dac51, prevented NR3C1-instigated excessive autophagy activation. Importantly, Dac51 effectively alleviated impaired insulin secretion and glucose intolerance in hyperglycemic β-cell specific NR3C1 overexpression mice. Our results determine that the NR3C1-FTO-m^6A modifications-*Atg* genes axis acts as a key mediator of balanced autophagic flux in pancreatic β-cells, which offers a novel therapeutic target for the treatment of diabetes.

Abbreviations: 3-MA: 3-methyladenine; AAV: adeno-associated virus; Ac: acetylation; Ad: adenovirus; AL: autolysosome; ATG: autophagy related; AUC: area under curve; Baf A1: bafilomycin A_1; βNR3C1 mice: pancreatic β-cell-specific NR3C1 overexpression mice; cFBS: charcoal-stripped FBS; Ctrl: control; ER: endoplasmic reticulum; FTO: fat mass and obesity associated; GC: glucocorticoid; GRE: glucocorticoid response element; GSIS: glucose-stimulated insulin secretion assay; HFD: high-fat diet; HG: high glucose; HsND: non-diabetic human; HsT2D: type 2 diabetic human; i.p.: intraperitoneal injected; KSIS: potassium-stimulated insulin secretion assay; m^6A: N6-methyladenosine; MeRIP-seq: methylated RNA immunoprecipitation sequencing; NR3C1/GR: nuclear receptor subfamily 3, group C, member 1; NR3C1-Enhc.: NR3C1-enhancement; NC: negative control; Palm.: palmitate; RNA-seq: RNA sequencing; T2D: type 2 diabetes; TEM: transmission electron microscopy; UTR: untranslated region; WT: wild-type.

ARTICLE HISTORY
Received 22 August 2022
Revised 20 March 2023
Accepted 4 April 2023

KEYWORDS
Autophagy; diabetes; FTO; NR3C1; m^6A; pancreatic β-cell

Introduction

Diabetes is a worldwide epidemic characterized by insulin resistance and pancreatic β-cell failure. Although the specific mechanism for the onset of diabetes is still unclear, numerous studies have implicated that pancreatic β-cell failure features all types of diabetes. In fact, β-cells are among the most important tissues dictating the final outcome of glucose control and the eventual development of diabetes. The occurrence of hyperglycemia and hyperlipidemia, which results in glucolipotoxicity for pancreatic islets, gradually diminishes β-cell mass and secretory capacity and exacerbates the diabetes [1]. Therefore, maintaining normal β-cell function is imperative in overall glucose homeostasis.

Macroautophagy/autophagy is a catabolic process of the lysosomal degradation of cellular components, which has long been demonstrated to control β-cell physiology and insulin secretory function in response to metabolism [2–4]. A set of~16–20 core *Atg* (autophagy related) genes [5] tightly regulates specific stages of autophagosome initiation or formation. In β-cells, there seems to be a consensus regarding the homeostatic role of autophagy in that it eliminates damaged organelles and unnecessary proteins to regulate the appropriate insulin response to glucose challenge, and to avoid β-cell apoptosis [2]. Interestingly, increasingly more studies have recently revealed the double-edged effect of autophagy in β-cells and diabetes. Even though physiologically enhanced autophagy improves the ability of β-cells to handle metabolic stress, hyperactive autophagic progression leads to β-cell damage and death that contributes to loss of functional β-cell mass in diabetes [6–15]. Overinduction of autophagy in β-cells leads to excessive digestion and degradation of essential cellular components, including insulin granules, mitochondria and endoplasmic reticulum (ER) membranes that lacks stringent substrate specificity, which results in significantly low insulin production and β-

CONTACT Xiao Han hanxiao@njmu.edu.cn; Fang Chen chenfang@njmu.edu.cn Key Laboratory of Human Functional Genomics of Jiangsu Province, Nanjing Medical University, 101 Longmian Avenue, Nanjing 211166, China
Supplemental data for this article can be accessed online at https://doi.org/10.1080/15548627.2023.2200625.

cell death. In type 2 diabetes (T2D) patients, dead β-cells with massive autophagic vacuole overload and no major chromatin condensation (signs of autophagy-associated cell death) were 4 times that of nondiabetic subjects [12]. Nevertheless, the causes and mechanisms of excessive autophagy in diabetic β-cells are poorly understood.

Glucocorticoids (GCs) are the prominent diabetogenic hormones since GCs excess under several pathophysiological conditions predisposes to T2D development [16–18]. In addition to the liver, β-cells are also important targets for the diabetogenic effects of GCs since excessive GC exposure inhibits insulin output, β-cell survival and proliferation via NR3C1/glucocorticoid receptor (nuclear receptor subfamily 3, group C, member 1) that widely expressed in pancreatic islet [19–25]. At the cellular level, NR3C1 locates in the cytoplasm in an unbound form and translocated into the nucleus upon binding to endogenous steroid hormone cortisol or exogenous glucocorticoid drugs, for example, dexamethasone; it also serves as one transcription factor for activating genes via the glucocorticoid response elements (GREs). Notably, ours and other studies have determined that deteriorative effect of aldosterone excess (a mineralocorticoid hormone) on β-cells is also mediated mainly by the NR3C1 rather than the NR3C2/mineralocorticoid receptor [26–30]. Accordingly, β-cell-specific NR3C1 overexpression results in insufficient insulin secretion, and then hyperglycemia and impaired glucose tolerance [31,32]. However, in contrast to the widely accepted deleterious effect of enhanced GC signaling, the molecular determinants of NR3C1 expression in β-cells are poorly understood. Also, the pivotal mechanism underlying NR3C1-enhancement induced β-cell dysfunction has not been fully elucidated either.

In this study, we demonstrate that NR3C1 is activated in β-cells exposed to glucolipotoxicity, which promotes deleterious β-cell hyperactive autophagy and diabetes. Using RNA sequencing (RNA-seq) and methylated RNA immunoprecipitation sequencing (MeRIP-seq), we documented that NR3C1-enhancement upregulated *N6*-methyladenosine (m^6A) RNA demethylase FTO (fat mass and obesity associated) protein expression, which caused diminished m^6A modifications on mRNAs of several *Atg* genes (*Atg12*, *Atg5*, *Atg16l2*, *Atg9a*). The *Atg* transcripts that lost m^6A were stabilized and triggered β-cell excessive autophagy, ultimately resulting in impaired insulin secretion and massive β-cell loss. Notably, the specific FTO inhibitor Dac51 effectively prevented dysregulated autophagy and rescued NR3C1-induced β-cell failure, hyperglycemia, and glucose intolerance in diabetes.

Results

Glucolipotoxicity promotes NR3C1 activation in β-cells

NR3C1 activity and expression patterns remained poorly understood in diabetic β-cells before. In present studies, we surprisingly observed that NR3C1 expression was ubiquitously increased in islets obtained from T2D patients, diet-induced diabetic mice and hyperglycemic *db/db* mice (Figure 1A-B). Furthermore, we detected that those isolated human islets with prolonged exposure to high glucose (HG) and palmitate (Palm.) similarly showed obviously NR3C1 upregulation compared with the control group, which was not observed in the pure HG- or Palm.-treated group (Figure 1C, S1A). NR3C1 nuclear translocation in β-cells were simultaneously provoked in T2D subjects as well as in the HG and Palm. treatment groups (Figure 1D-F), which were almost closed to what we observed in the human islets and MIN6 cells treated with dexamethasone or aldosterone (Figure S1B – E), both of which serve as NR3C1 agonists in pancreatic β-cells [26,33]. Using luciferase reporter assay, we confirmed that chronic HG and Palm. induced the nuclear transcriptional regulatory activity of NR3C1, but only in the presence of NR3C1 ligands (endogenous or exogenous) in the medium culture, suggested that glucolipotoxicity upregulates NR3C1 levels to enhance GC sensitivity in β-cells (Figure 1G).

We investigated the reason for glucolipotoxicity-induced excessive NR3C1 in the β-cells. Since histone acetylation at NR3C1 exon I_7 promoter is associated with increased expression of NR3C1 [34,35], we measured the effect of chronic HG and Palm. on the histone H3 and H4 acetylation (H3Ac and H4Ac) at *Nr3c1* promoter I_7 by ChIP-qPCR. There was a 6-fold increase in H3Ac and 12.5-fold increase in H4Ac in MIN6 cells exposed to chronic HG and Palm. (Figure 1H-I). Surprisingly, increased chromatin accessibility at the *Nr3c1* promoter I_7 was observed meanwhile (Figure 1J). Consistently, total *Nr3c1* mRNA levels were significantly upregulated in MIN6 cells treated with chronic HG or Palm. (Figure 1K). Similar results were also observed in INS1 cells (Figure 1L-O). These results indicated that elevated NR3C1 expression in diabetic β-cells arose from enhanced H3Ac and H4Ac enrichment and chromatin accessibility. Taken together, the expression levels and activities of NR3C1 was continuously enhanced in β-cells in response to glucolipotoxicity.

Enhanced-NR3C1 leads to hyperactive autophagic progression in β-cells

Human islets perfusion analysis revealed that *NR3C1*-knockdown effectively reversed impaired β-cell secretion both at the 1st and 2nd phases in T2D human islets (Figure 2A and B, Figure S2A); glucose-stimulated or potassium-stimulated insulin secretion assays (i.e., GSIS and KSIS), insulin biosynthesis assays further indicated that *NR3C1*-knockdown could not only ameliorate defected insulin secretion, but also reversed impaired insulin synthesis (Figure 2C-F, **S2B)**, indicated that enhanced-NR3C1 is tightly associated with β-cell dysfunction in T2D patients. In islets, glucocorticoid signaling has been shown to regulate numerous processes, including insulin secretion, ion channel activity, cAMP signaling, proliferation and development [23,36–39]. Nevertheless, the mechanism associated with β-cell failure induced by excessive NR3C1 has not been thoroughly studied. Therefore, we assayed gene expression in the MIN6 cells transfected with NR3C1-overexpressing plasmids or empty vectors by RNA seq (Figure 2G). We then applied the Kyoto Encyclopaedia of Genes and Genomes algorithms (KEGG) and MSigDB software for gene set-enrichment analysis. The most enriched pathway among others according to ES score was autophagy pathway, in which 32 dysregulated genes were involved (Figure 2H and I, Table S1). We verified the RNA-seq results by qRT-PCR assays and found that numerous *Atg* genes, including *Atg10*, *Atg12*, *Atg5*, *Atg4*, *Atg9a, Wipi1, Atg16l2*, *Pik3c3*, were significantly upregulated in NR3C1 overexpressing β-cells (Figure 2J).

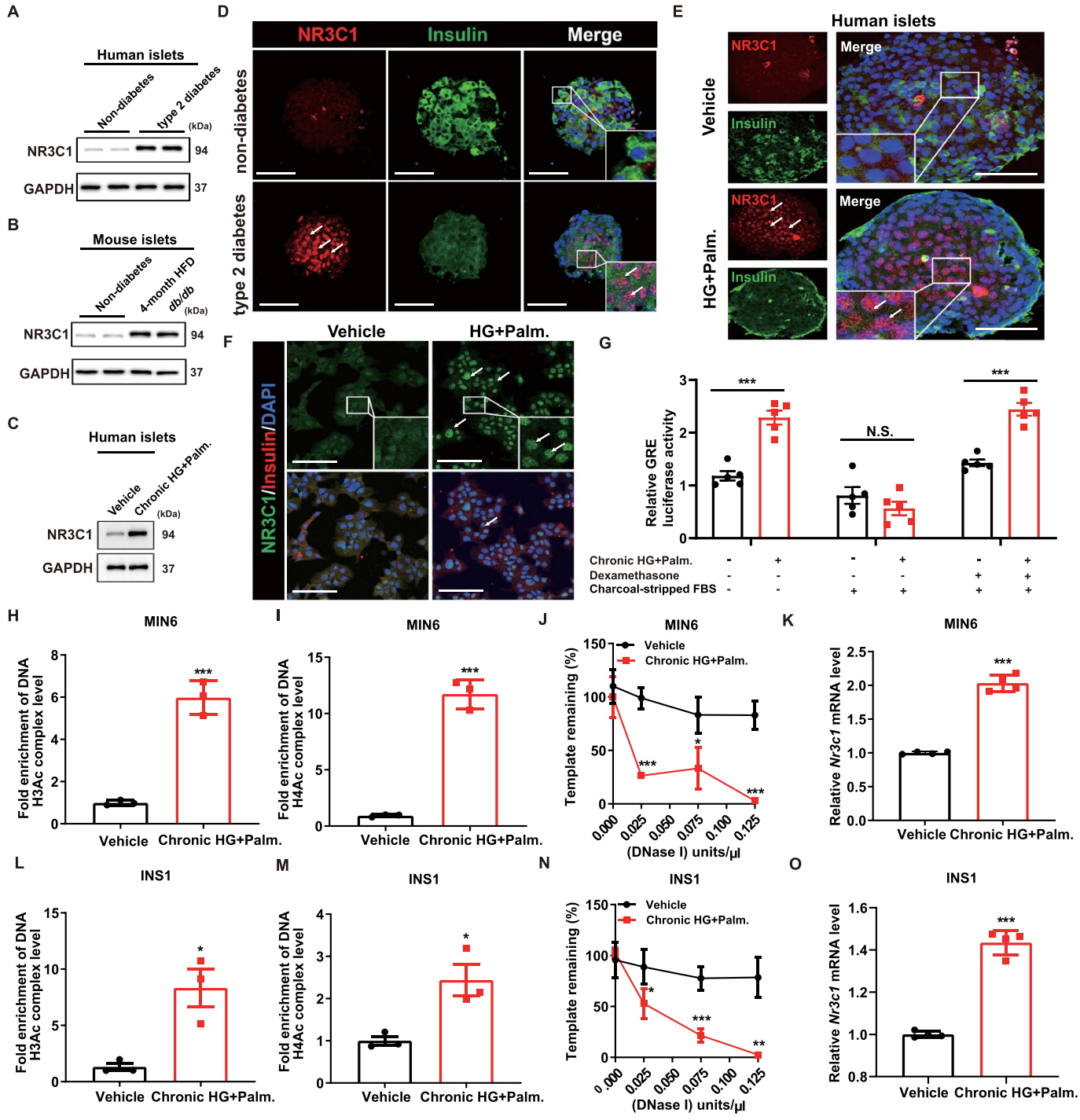

Figure 1. NR3C1 is continuously activated in pancreatic islets in response to glucolipotoxicity. (A and B) the protein levels of NR3C1 in T2D human islets, diet-induced diabetic mice and hyperglycemic db/db mice. GAPDH was used as internal control. (C) the protein levels of NR3C1 in human islets exposed to prolonged HG and Palm. GAPDH was used as internal control. (D) NR3C1 expression and localization in islets from donors of T2D and nondiabetic humans was confirmed via immunofluorescence. Insulin (green), NR3C1 (red), and DAPI (blue). Scale bar: 50 μm. (E) NR3C1 expression and localization in human islets exposed to prolonged HG and Palm. was confirmed via immunofluorescence. Insulin (green), NR3C1 (red), and DAPI (blue). Scale bar: 50 μm. (F) NR3C1 expression and localization in MIN6 cells treated with prolonged HG and Palm. was confirmed via immunofluorescence. Insulin (red), NR3C1 (green), and DAPI (blue). Scale bar: 50 μm. (G) MIN6 cells were transfected with Pgre-luc for 24 h and treated with chronic HG and Palm., then luciferase reporter assay was carried out. (H and I) ChIP-Qpcr analysis of the capacity of acetylation of histone H3 (H) and H4 (I) binding to the Nr3c1 promoter I_7 was performed in MIN6 cells exposed to prolonged HG and Palm. (J) Graphs depict the relative chromatin accessibility (the percentages of undigested DNA among template genomic DNA) in MIN6 cells exposed to prolonged HG and Palm. (K) Relative Nr3c1 mRNA levels in MIN6 cells exposed to prolonged HG and Palm. (L and M) ChIP-Qpcr analysis of the capacity of acetylation of histone H3 (L) and H4 (M) binding to the Nr3c1 promoter I_7 was performed in INS1 cells exposed to prolonged HG and Palm. (N) Graphs depict the relative chromatin accessibility in INS1 cells exposed to prolonged HG and Palm. (O) Relative Nr3c1 mRNA levels in INS1 cells exposed to prolonged HG and Palm. Data are presented as mean ± SEM. * $P < 0.05$, ** $P < 0.01$, *** $P < 0.001$ vs. Vehicle group.

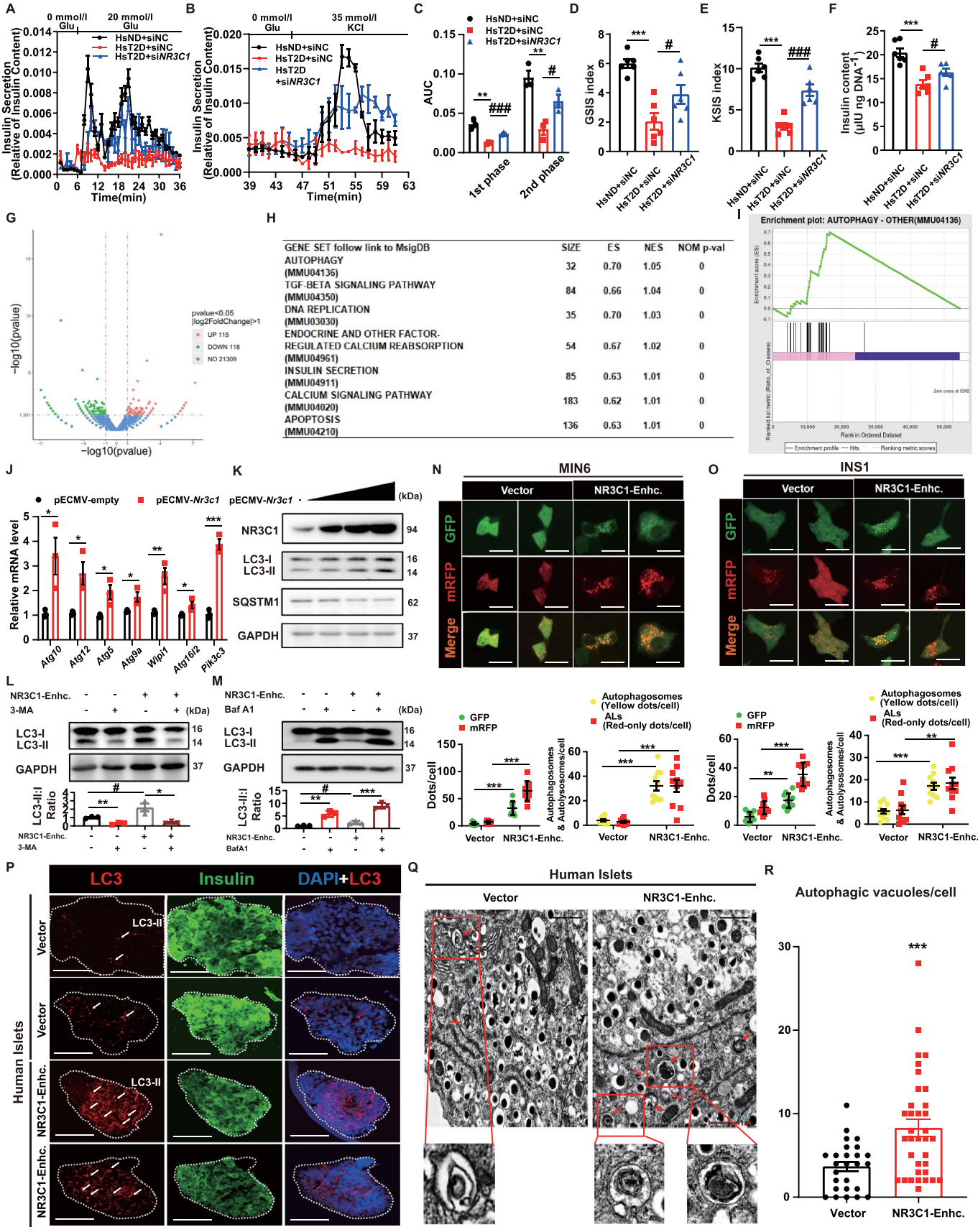

GENE SET follow link to MsigDB	SIZE	ES	NES	NOM p-val
AUTOPHAGY (MMU04136)	32	0.70	1.05	0
TGF-BETA SIGNALING PATHWAY (MMU04350)	84	0.66	1.04	0
DNA REPLICATION (MMU03030)	35	0.70	1.03	0
ENDOCRINE AND OTHER FACTOR-REGULATED CALCIUM REABSORPTION (MMU04961)	54	0.67	1.02	0
INSULIN SECRETION (MMU04911)	85	0.63	1.01	0
CALCIUM SIGNALING PATHWAY (MMU04020)	183	0.62	1.01	0
APOPTOSIS (MMU04210)	136	0.63	1.01	0

Figure 2. NR3C1 enhancement triggers hyperactive autophagy in pancreatic β-cells. (A – C) Isolated T2D (HsT2D) and non-diabetic human (HsND) islets that transfected with si-negative control (siNC) or siNR3C1 during islet perfusion assays in three separate experiments. AUC (area under curve) values for the 1st and 2nd phases of GSIS in islet perfusion were calculated in C. (D – F) GSIS and KSIS assays were performed for isolated HsT2D and HsND islets in A. GSIS and KSIS indices (GSI and KSI) were calculated in D and E. GSI and KSI refer to the ratio of glucose- or KCl-stimulated insulin secretion to basal insulin secretion. Insulin content was measured in F. ** $P < 0.01$, *** $P < 0.001$ vs. HsND islets + siNC group; # $P < 0.05$, ### $P < 0.001$ vs. HsT2D islets + siNC group. (G) Volcano plots of differential gene expressions in MIN6 cells transfected with NR3C1-overexpressing plasmids and empty vectors. (H) Gene set enrichment analysis (GSEA) according to identified using

To further confirm that whether NR3C1-enhancement stimulates unbalanced autophagy, we transfected NR3C1 overexpression plasmids into MIN6 and INS1 cells, and detected the expression for MAP1LC3B/LC3 (microtubule-associated protein 1 light chain 3 beta) and SQSTM1/p62 (a protein specifically degraded in lysosomes), which contribute to autophagosome formation and substrate degradation, respectively. NR3C1 overexpression caused an increase in LC3-II but a decrease in SQSTM1 protein levels dose-dependently (Figure 2K). Indeed, 3-methyladenine (3-MA, a PI3K and PtdIns3K inhibitor) or bafilomycin A_1 (Baf A1, a vacuolar-type H+-translocating ATPase inhibitor) treatment experiment further confirmed that NR3C1 enhancement promoted the activation of autophagy (Figure 2L and M). Besides, in MIN6 (Figure 2N) and INS1 (Figure 2O) cells-expressing tandem mRFP-GFP-LC3, increased autophagosomes (yellow dots) and autolysosomes (AL, red-only dots) demonstrated that autophagy flux was enhanced in NR3C1-overexpressing β-cells. Hyperactive autophagy was also observed in NR3C1-overexpressed human islets (Figure 2P), and increased number of autophagic structures in β-cells was measured by transmission electron microscopy (TEM) meanwhile (Figure 2Q and R).

Glucolipotoxicity-activated NR3C1 deteriorates β-cell function and survival via excessive autophagy

Accumulation of autophagic vacuoles and autophagosomes in diabetic β-cells, as well as increased dead β-cells with vacuole engulfment, contribute to β-cell dysfunction in diabetes [12]. According to our observations, prolonged exposure to HG and Palm. significantly stimulated hyperactive autophagic flux in MIN6 and INS1 cells, which could be retrieved by *Nr3c1*-knockdown (Figure 3A-D, S2C – E, S3A – B). However, NR3C1 inhibition did not disturb enhanced autophagy arose from pure glucotoxicity or lipotoxicity (Figure S3C – D). Surprisingly, autophagy inhibition (achieved by 3-MA, Baf A1 or *Atg5* or *Atg7*-knockdown) reversed impaired insulin secretion and/or insulin content arose from glucolipotoxicity (Figure 3E and F, S3E – H), while neither 3-MA or Baf A1 rescue pure lipotoxicity-induced impaired insulin secretion (Figure S3I – L), indicates that hyperactive autophagy is harmful for β-cell fate under glucolipotoxic but not lipotoxic conditions. More importantly, *Nr3c1*-knockdown similarly rescued β-cell failure in glucolipotoxic conditions (Figure 3E and F). As expected, autophagy inhibition effectively alleviated impaired insulin secretion and insulin content in NR3C1-overexpressed MIN6 cells (Figure 3G-J), and β-cell apoptosis (Figure 3K). Collectively, NR3C1-enhancement induced excessive autophagy to instigate defected insulin secretion and increased β-cell apoptosis in glucolipotoxic conditions.

NR3C1 activation lessens Atg genes m^{6}A methylation in β-cells

We then explored the molecular mechanism underlying excessive autophagy in NR3C1-enhanced β-cell. According to our observations, NR3C1 overexpression dramatically downregulated the total m^{6}A in β-cells (Figure 4A). The pattern of m^{6}A distribution in NR3C1-overexpressing β-cells was further determined with MeRIP-seq which is an immunocapturing approach for the unbiased transcriptome-wide localization of m^{6}A in high resolution. Gene ontology (GO) analysis revealed that NR3C1 enhancement-induced alterations in m^{6}A modification were significantly ($p < 0.05$) enriched in genes involved in autophagy process, alongside other biological processes that were critical for β-cell function, such as response to glucose, exocytosis, and regulation of apoptotic signaling pathway (Figure 4B). Combined with the transcriptomics results shown in Figure 2G-J, it was indicated that NR3C1 enhancement-induced hyperactive β-cell autophagy is highly-possibly related with m^{6}A-methylation status on mRNAs of *Atg* genes.

We deeply analyzed MeRIP-seq and found that declined m^{6}A was detected in a plenty of mRNAs associated with autophagy (**Table S2**). Among them, we paid more attention to *Atg12, Atg5, Atg9a, Atg16l2*, since MeRIP-seq and RNA-seq in NR3C1-overexpressing MIN6 cells showed declined m^{6}A modifications in those 4 *Atg* genes, while their expression levels were remarkedly increased, indicating that *Atg12, Atg5, Atg9a, Atg16l2* may play more important roles in the NR3C1-m^{6}A modulating β-cell autophagy. Analysis of MeRIP-seq data revealed 4 decreased m^{6}A modifications within 3'-untranslated region (UTR) of *Atg12* transcript (Figure 4C), and 1 decreased m^{6}A peak was observed in the *Atg5*, *Atg16l2*, and *Atg9a* transcripts, respectively, which was also located in the 3'-UTR (Figure 4D-F).

m^{6}A RNA demethylase FTO is responsible for NR3C1-upregulated Atg genes

To ascertain the reason for diminished m^{6}A modifications on those autophagic mRNAs, we detected genes expression associated with m^{6}A demethylation (*Alkbh5*, *Fto*), m^{6}A reader (*Ythdc1, Ythdf1*, *2*, *3*) and m^{6}A methyltransferase (*Mettl3*, *Mettl14*, *Wtap*) in NR3C1-overexpressing MIN6 cells,

MSigDB software. (I) GSEA enrichment plot of autophagy pathway. (J) the mRNA levels of Atg genes in NR3C1-overexpressing plasmids and vector-transfected MIN6 cells. (K) MIN6 cells were transfected with different concentrations of NR3C1 overexpression plasmids, and then the protein levels of LC3 and SQSTM1 were measured by western blot. GAPDH was used as internal control. (L) Western blot analysis of LC3 in control and NR3C1-overexpressed cells treated with or without 10 mmol/l 3-MA for 4 h. (M) Western blotting analysis of LC3 in control and NR3C1-overexpressed cells treated with or without 5 nmol/l Baf A1 for 2 h. (N) MIN6 cells were transfected with Mrfp-GFP-LC3 adenovirus with or without NR3C1-overexpression for 24 h. Cells were observed to distinguish between autophagosome (yellow puncta) and autolysosome (AL, red-only puncta) after colocalization analysis using a confocal microscope and the dots per cell were quantified below ($n = 10$). Scale bar: 20 μm. (O) INS1 cells were transfected with Mrfp-GFP-LC3 adenovirus with or without NR3C1-overexpression for 24 h. The dots per cell were quantified below ($n = 10$). Scale bar: 20 μm. (P) Human islets were transfected with Ad-NR3C1 or Ad-GFP for 24 h. LC-3 in pancreatic β-cells was confirmed via immunofluorescence. Insulin (green), LC3 (red), and DAPI (blue). Scale bar: 50 μm. (Q and R) Representative TEM images of human pancreatic β-cells transfected with Ad-NR3C1 or Ad-GFP. Arrows indicate autophagic structures. The graphs in R show quantification of autophagic structures in β-cells in Q ($n = 26–35$). Scale bar: 1 μm. Data are presented as mean ± SEM. For J, L – O, R, * $P < 0.05$, ** $P < 0.01$, *** $P < 0.001$ vs. empty vector group.

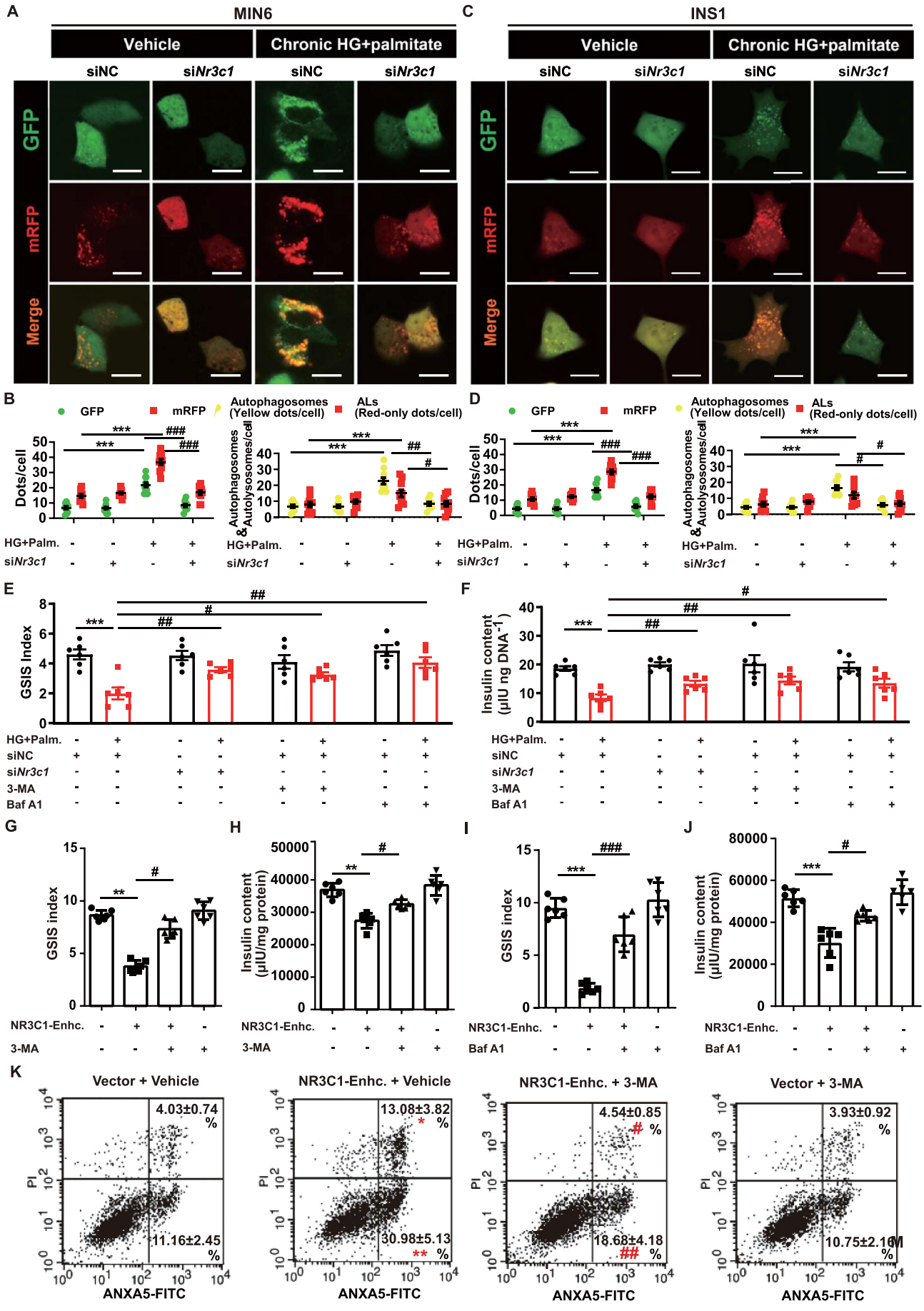

Figure 3. Glucolipotoxicity-activated NR3C1 deteriorates β-cell function and survival via excessive autophagy. (A and B) Nr3c1-knockdown or control MIN6 cells were transfected with Mrfp-GFP-LC3 adenovirus with or without prolonged HG and Palm. Cells were observed to distinguish between autophagosome (yellow puncta) and AL (red-only puncta) after colocalization analysis using a confocal microscope and the dots per cell were quantified in B ($n = 10$). Scale bar: 20 μm. (C and D) Nr3c1-

among which m^{6}A RNA demethylase *Fto* was dramatically elevated (Figure 5A). Western blot and immunofluorescence assays further verified elevated FTO expression in NR3C1-enhanced MIN6 cells and human islets (Figure 5B and C). Using ChIP and luciferase reporter assay, we observed that NR3C1 bind to *Fto* gene promoter at three sites and positively regulated its transcriptional promoter activity (Figure 5D and E), indicating that *Fto* contains GREs, which makes it able to serve as a NR3C1 target gene.

FTO is the first identified RNA demethylase that catalyses m^{6}A demethylation in an Fe (II)- and α-ketoglutarate-dependent manner [40]. m^{6}A demethylation influences all fundamental aspects of mRNA metabolism, including mRNA stability, translation, subcellular localization and alternative splicing [41–43]. Given that FTO is an m^{6}A "eraser" of RNA methylation and regulates the expression of genes through modification of methylation-demethylation states of mRNAs, we next investigated whether FTO is responsible for diminished m^{6}A modifications on those 4 *Atg* genes (i.e., *Atg12, Atg5, Atg9a, Atg16l2*) that deeply involved in the NR3C1-m^{6}A regulating β-cell autophagy. RT-qPCR and MeRIP-qPCR assays showed that *Fto*-knockdown dramatically abolished the upregulation of *Atg12, Atg5, Atg9a, Atg16l2* in NR3C1-overexpressing MIN6 cells (Figure 5F), while it eliminated NR3C1-induced declined m^{6}A levels on these autophagic transcripts (Figure 5G), which fully indicated that NR3C1-FTO mediates the mRNA demethylation of these *Atg* genes and triggers their highly expression. To further assess whether m^{6}A modifications on these *Atg* genes mRNAs were necessary for NR3C1-FTO axis-mediated gene expression, we then constructed wild-type (WT) and m^{6}A consensus sequence mutant (A-to-T mutation, MUT) *Atg12*, *Atg5*, *Atg16l1*, *Atg9a*-3"UTR luciferase reporters (Figure 5H). NR3C1 overexpression obviously promoted luciferase activity of the reporter constructs containing WT 3"UTR of those *Atg* genes, which was abrogated when *Fto* was knockdown or the indicated m^{6}A modification sites were mutated (Figure 5I-L). m^{6}A modifications exert effects on many aspects of gene expression, including mRNA stability, nuclear export, alternative pre-mRNA splicing etc. RT-qPCR results showed that NR3C1-FTO axis prevented the rapid decay of almost all 4 *Atg* gene mRNAs (Figure 5M-P), which indicated that NR3C1-FTO axis-mediated demethylation is implicated in those 4 *Atg* gene mRNAs degradation. Together, NR3C1-FTO axis upregulated *Atg12*, *Atg5*, *Atg9a*, and *Atg16l2* expression via modulating their mRNA stability.

We continued to confirm that whether FTO indeed participates in hyperactive autophagy in NR3C1-enhanced β-cells. Western blot assays showed that FTO deletion remarkedly weakened the increased ratio of LC3-II:I, decreased SQSTM1 expression and excessive autophagic flux induced by NR3C1-overexpression (Figure 5Q and R). All these observations implicated that FTO targets *Atg12*, *Atg5*, *Atg9a*, and *Atg16l2* transcripts and mediates their expression in an m^{6}A-dependent manner, and further regulates autophagy in NR3C1-enhanced β-cells.

Specific inhibition of FTO alleviates NR3C1 activation-induced β-cell dysfunction and hyperactive autophagy

To further verify that whether FTO demethylates those autophagic transcripts thus leading to hyperactive autophagy and then β-cell failure in NR3C1-enhanced models, we applied Dac51 in our subsequent research (Figure 6A), which has recently been tested as a more potent FTO inhibitor that dampens FTO demethylation activity [44]. As shown in Figure 6B-F, Dac51 inhibited hyperactivation of autophagy in NR3C1-overexpressed MIN6 and INS1 cell. As GSIS assays results shown in Figure 6G-H and S4A – B, defective insulin secretion and insulin content in NR3C1-enhanced β-cells could be also dose-dependently restored by Dac51. Parallel to this, human islets perfusion analysis showed that NR3C1-enhanced β-cell secreted less insulin both at the 1st and 2nd phases, which could be partially reversed by Dac51 (Figure 6I and J). Moreover, Dac51 ameliorated decreased viability of NR3C1-enhanced MIN6 cells (Figure 6K and S4C), while TUNEL assays proved that Dac51 reduced β-cell apoptosis in NR3C1-enhanced human islets (Figure 6L). Notably, the protective effect of Dac51 on NR3C1-stimulated impaired insulin secretion (Figure S4D – E) and increased cell apoptosis (Figure S3F) was almost abolished in mouse islets treated with carbamazepine (CBZ, an autophagy activator). Collectively, these results confirmed that FTO-mediated autophagic transcripts demethylation was responsible for hyperactive autophagy and β-cell failure in NR3C1-enhanced models.

Dac51 treats impaired insulin secretion and hyperglycemia in β-cell-specific NR3C1 overexpression mice

To further evaluate the effect of Dac51 on impaired glucose metabolism induced by NR3C1-enhancement in β-cells, we obtained mice with increased NR3C1 expression restricted to their β-cells were via pancreatic intraductal AAV-*RIP2-Nr3c1–3×Flag* infusion, hereafter named β-cell-specific NR3C1 overexpression (βNR3C1) mice. The effective delivery of virus and NR3C1 enhancement were confirmed (Figure 7A and B). Then, all operated mice were randomized into 5 groups: control mice (AAV-vectors infected, Ctrl) intraperitoneal injected (i.p.) with 2 mg/kg Dac51 or PBS, βNR3C1 mice (AAV-*RIP2-Nr3c1* infected) i.p. with 2 mg/kg Dac51, 0.5 mg/kg Dac51 or PBS, and experiments were scheduled to

knockdown or control INS1 cells were transfected with Mrfp-GFP-LC3 adenovirus with or without prolonged HG and Palm. The dots per cell were quantified in D (n = 10). Scale bar: 20 μm. (E and F) MIN6 cells were treated as indicated, and then GSIS (E) and insulin content (F) was determined. (G and H) MIN6 cells were transfected with NR3C1 overexpression plasmids for 24 h and treated with or without 10 mmol/l 3-MA for 4 h., and then GSIS (G) and insulin content (H) was determined. (I and J) MIN6 cells were transfected with NR3C1 overexpression plasmids for 24 h and treated with or without 5 nmol/l Baf A1 for 2 h, and then GSIS (I) and insulin content (J) was determined. (K) After pretreated with 3-MA (10 μmol/l) for 2 h, MIN6 cells were transfected with NR3C1 overexpression plasmids for an additional 72 h, and then flow cytometry assay was performed. Data are presented as mean ± SEM. For B – F, *** $P < 0.001$ vs. vehicle + siNC group; # $P < 0.05$, ## $P < 0.01$, ### $P < 0.001$ vs. HG + Palm. + siNC group. For G – K, * $P < 0.05$, ** $P < 0.01$, *** $P < 0.001$ vs. vehicle + empty vector group; # $P < 0.05$, ## $P < 0.01$, ### $P < 0.001$ vs. vehicle + NR3C1-Enhc. group.

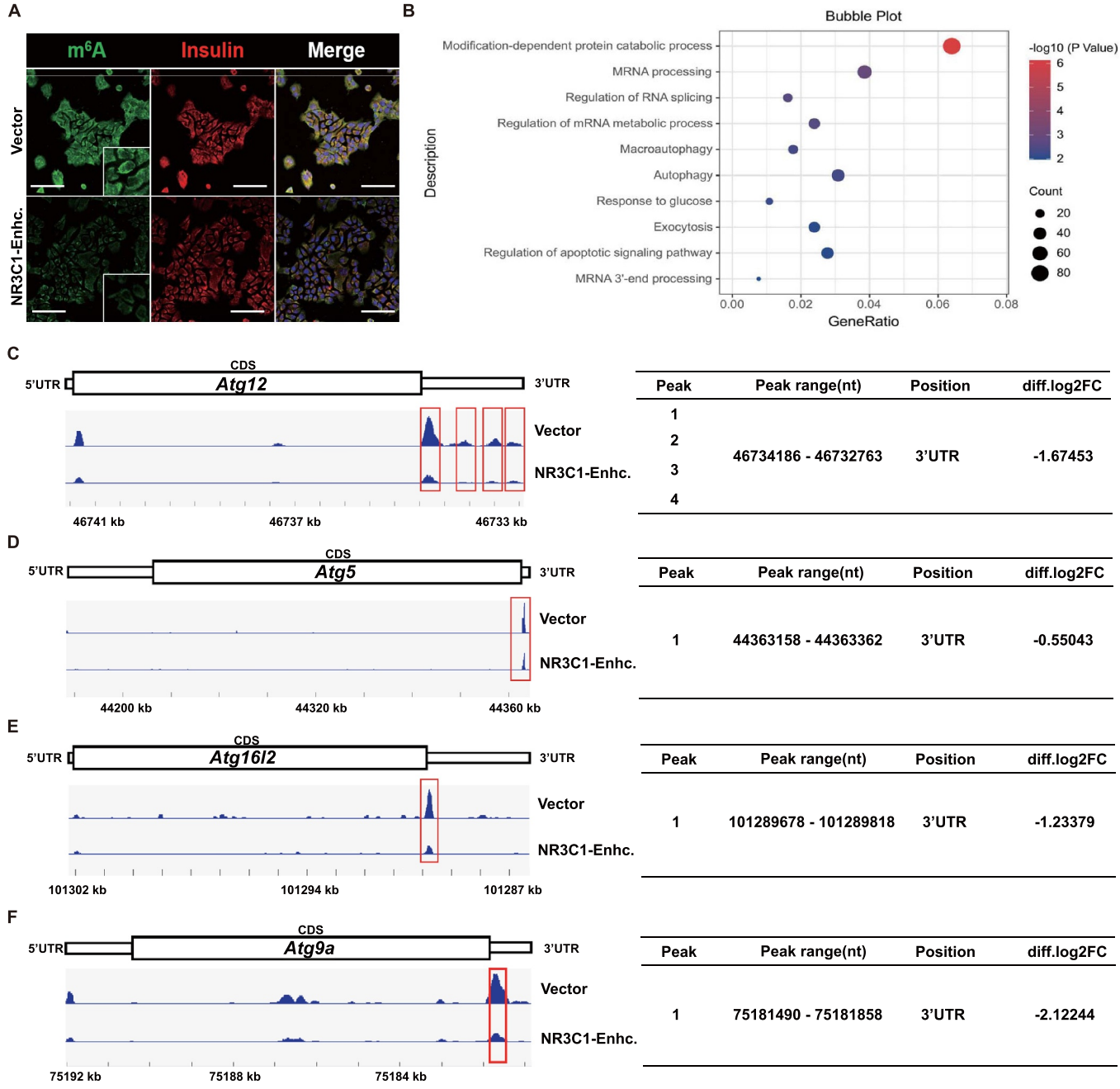

Peak	Peak range(nt)	Position	diff.log2FC
1 2 3 4	46734186 - 46732763	3'UTR	-1.67453

Peak	Peak range(nt)	Position	diff.log2FC
1	44363158 - 44363362	3'UTR	-0.55043

Peak	Peak range(nt)	Position	diff.log2FC
1	101289678 - 101289818	3'UTR	-1.23379

Peak	Peak range(nt)	Position	diff.log2FC
1	75181490 - 75181858	3'UTR	-2.12244

Figure 4. NR3C1 enhancement lessens Atgs m^{6}A methylation in β-cells. (A) Immunofluorescent staining in MIN6 cells transfected with empty or NR3C1-overexpressing vectors was performed for m^{6}A (green), insulin (red), and DAPI (blue). Scale bar: 40 μm. (B) Gene ontology analysis of MeRIP-seq in NR3C1-overexpressing MIN6 cells. (C – F) Integrative genomics viewer (IGV) plots of m^{6}A peaks at the Atg12 (C), Atg5 (D), Atg16l2 (E) and Atg9a (F). The horizontal axis shows sequence reads of the mRNA region of each peak, and the vertical axis represents the absolute number of m^{6}A modification sites. The bars above each gene plot represent the location of each peak according to genomic DNA sequence. The red boxes indicate m^{6}A peaks on the Atg12, Atg5, Atg16l2 and Atg9a transcripts, and the position of the peaks on the mRnas are shown on the right side of each panel. CDS: coding sequence.

determine the effects of Dac51 on βNR3C1 mice (Figure 7C). βNR3C1 mice i.p. with PBS alone showed remarkably elevated blood glucose levels and impaired glucose tolerance regardless of unaffected insulin sensitivity (Figure S5A – D), as previously reported [19,32]. During Dac51 administration, no significant changes were observed in body weight (Figure 7D) and insulin sensitivity (Figure S5E – F) between groups. In contrast, βNR3C1 mice i.p. with Dac51 gradually improved their diabetes-related phenotypes (especially in the high-dose group), manifested as declined blood glucose (Figure 7E-G) and lessened glucose intolerance at 13 weeks and 16 weeks of age (Figure 7H-K), while no between-group changes were noted in Ctrl mice i.p. with Dac51 or PBS. Consistently, insulin secretion levels revealed a marked rebound in βNR3C1 mice with Dac51 administration (Figure 7L). Notably, Dac51 did not interfere with NR3C1 expression or translocation in βNR3C1 mice (Figure S5G). We continued to assess the effects of Dac51 on β-cell function of βNR3C1 mice by *ex vivo* islet perfusion assays. NR3C1-enhancement significantly inhibited high-glucose-coupled

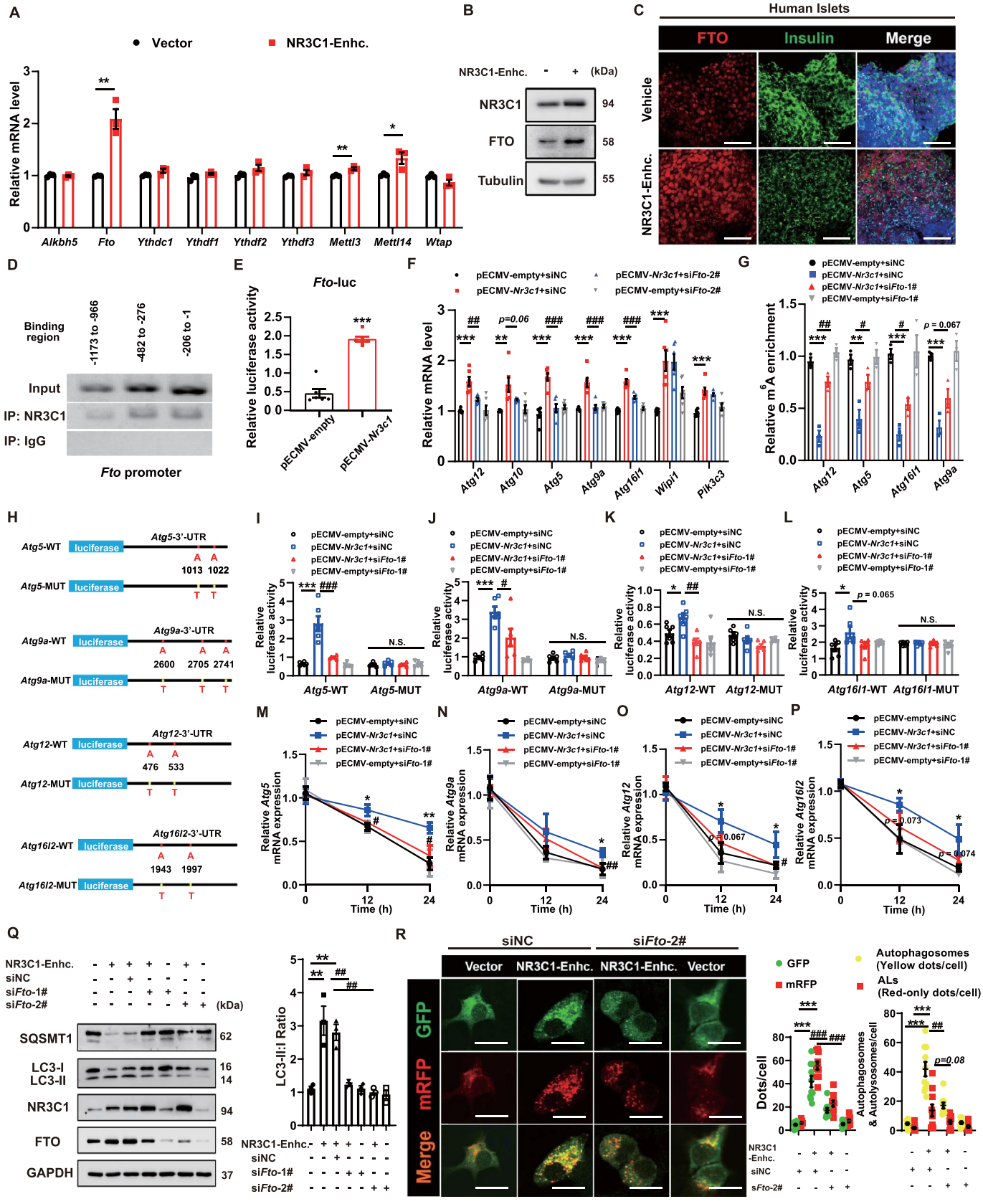

Figure 5. m^{6}A RNA demethylase FTO is responsible for NR3C1-induced hyperactive autophagy. (A) the mRNA levels of genes associated with m^{6}A modifications in NR3C1-overexpressing MIN6 cells. (B) the protein level of FTO in MIN6 cells in A. GAPDH was used as internal control. (C) Human islets were transfected with Ad-NR3C1 for 24 h. FTO expression in pancreatic β-cells was confirmed via immunofluorescence. Insulin (green), FTO (red), and DAPI (blue). Scale bar: 30 μm. (D and E) ChIP and luciferase reporter assay confirmed that NR3C1 bind to Fto promoter on three sites and upregulated its transcriptional activity. (F) the levels of autophagic mRnas in MIN6 cells transfected with NR3C1-overexpressing plasmids and siFto. (G) MeRIP-Qpcr analysis of m^{6}A levels of Atg12, Atg5, Atg16l2 and Atg9a mRNA in MIN6 cells transfected with NR3C1-overexpressing plasmids and siFto. (H) Schematic diagram of luciferase reporter constructs. (I – L) Relative luciferase activity of wild-type (WT) or mutant (A-to-T mutation, MUT) Atg5 (I), Atg9a (J), Atg12 (K), and Atg16l2-3′UTR luciferase reporter (L) in MIN6 cells transfected with NR3C1-

insulin secretion which specifically reversed by Dac51 administration (Figure 8A and B). Besides, we noticed that Dac51 also effectively protected β-cells from NR3C1-induced apoptosis *in vivo* (Figure 8C), which paralleled what we observed in human primary islets *ex vivo*. Collectively, FTO inhibition exerted a robust effect on the treatment for NR3C1 enhancement-induced impaired glucose metabolism.

We next verified whether autophagy regulation mediates the rescue of NR3C1-FTO axis-induced β-cell dysfunction and apoptosis by Dac51 *in vivo*. In βNR3C1 mice, as expected, NR3C1 overexpression increased the number of LC3-II-positive and SQSTM1-negative β-cells in pancreas. Surprisingly, Dac51 administration similarly attenuated the enhanced autophagic flux in βNR3C1 mice (Figure 8D and E), as it did in NR3C1-enhanced β-cells *in vitro*. TEM images from β-cells for βNR3C1 mice also demonstrated accumulation of autophagic vacuoles, which were similarly alleviated after Dac51 treatment (Figure 8F). In summary, autophagy regulation played essential roles in Dac51 rescue of NR3C1-induced β-cell failure and diabetes.

Discussion

In this current study, we explored the role of hyperstimulated autophagy in β-cell dysfunction and apoptosis under glucolipotoxic conditions. Increased NR3C1 expression and nuclear-translocation in human and rodent pancreatic β-cells correlated with excessive autophagy progression detrimental to β-cell fate in glucolipotoxic status. Mechanically, NR3C1-enhancement stimulated FTO expression which induced autophagic transcripts hypomethylation (mainly *Atg12*, *Atg5*, *Atg16l2* and *Atg9a*), leading to hyperactive autophagy and β-cell failure. Dac51, the specific FTO inhibitor, reversed NR3C1-induced excessive autophagy, which rescue β-cell failure.

Autophagy plays complicated roles in β-cell mass and function. On the one hand, as an intracellular catabolic system, autophagy is essential in the basal turnover of organelles and maintenance of function in β-cells, β-cells that lack of key *Atg* gene expression (e.g., *Atg5*, *Atg7*) fail to address stress conditions that could lead to abnormal insulin secretion and overt diabetes [45,46]; On the other, both earlier and recent studies described a possible involvement of autophagy in β-cell death in conditions such as PDX1 deficiency [14]. Alloxan, streptozotocin or rapamycin-mediated stimulation of autophagy also impairs islet function and survival [15,47], whereas the precise mechanism is not explained. Combined that dead β-cells with signs of autophagy-associated cell death are significantly increased in T2D patients [12], it is reasonable that hyperstimulation of autophagy in β-cells has a negative effect, but how and when it occurs in the progression of diabetes has not been clear.

Here we described that deleterious autophagy overlord happened upon NR3C1 activation in β-cells under glucolipotoxic conditions. We found that glucolipotoxicity epigenetically upregulated NR3C1 expression, which enhanced GC sensitivity of β-cells in that inductive NR3C1 transactivation activity was observed even without the addition of exogenous NR3C1 agonists. Both oxidative stress and ER stress is deeply involved in β-cell failure under glucolipotoxic conditions. We investigated that thapsigargin-mimicked ER stress stimulated NR3C1 expression and its transcriptional activity in β-cells in a dose-dependent manner, while oxidative stress (mimicked by H_2O_2) had no such effect (**Figure S1F – H**), indicates that ER stress-induced by glucolipotoxicity may lead to abnormally elevated NR3C1 activity in β-cells. When NR3C1 was continuously enhanced, β-cells displayed hyperactive autophagic progression. Even though some studies describe a protective role of enhanced autophagy in β-cell-combating stress [48,49], our findings reveal that enhanced autophagy induced by NR3C1-enhancement exerted harmful effects on β-cells in response to nutrient overload conditions. For one thing, 3-MA and Baf A1, both of which inhibit specific phases of autophagy flux, similarly rescue NR3C1-stimulated impaired insulin secretion and β-cell loss. For another, *Nr3c1*-knockdown or autophagy inhibition braked excessive autophagy flux, accompanied with improved β-cell function in glucolipotoxic status. Obviously, although former studies imply that autophagy is activated as an adaptive response and provides β-cells with a safety mechanism to eliminate damaged mitochondria and/or unnecessary proteins to avoid dysfunction and apoptosis in glucotoxic or lipotoxic conditions [50], hyperstimulation of autophagy plays opposite roles in β-cells that exposed to glucolipotoxicity. The concept of glucolipotoxicity refers to the combined, deleterious effects of elevated glucose and fatty acid levels on β-cells function and survival [51]. Compared with purely glucotoxicity or lipotoxicity, glucolipotoxicity is more appropriate to describe damaging or toxic effects on the β-cells in diabetic status, not only due to the commonly occurred hyperglycemia and hyperlipidemia in the development of diabetes, but also the fact that lipotoxicity is dependent on elevated glucose levels indeed [52]. At the level of β-cells, glucolipotoxicity plays a major role during the decompensation phase [52]. Thus, we predict that excessive autophagic progression instigated by glucolipotoxicity at least occur frequently in the middle and late stages of diabetes progression, which exerts negative effects on β-cell fate and eventually evolves toward β-cell decompensation and. However, there is still a lack of dynamic monitoring of β-cell autophagic flux in diabetic models to support this.

overexpressing plasmids and siFto. Firefly luciferase activity was measured and normalized to Renilla luciferase activity. (M – P) MIN6 cells transfected with NR3C1-overexpressing plasmids and siFto were treated with actinomycin D (10 μg/ml) for the indicated times. The expression of Atg5 (M), Atg9a (N), Atg12 (O), and Atg16l2 (P) was analyzed by Qrt-PCR. (Q) the protein levels of LC3 and SQSTM1 in MIN6 cells transfected with NR3C1-overexpressing plasmids and siFto. GAPDH was used as internal control. (R) MIN6 cells in Q were further transfected with Mrfp-GFP-LC3 adenovirus to distinguish between autophagosome (yellow puncta) and AL (red puncta) after colocalization analysis using a confocal microscope and the dots per cell were quantified on the right ($n = 10$). Scale bar: 20 μm. Data are presented as mean ± SEM. For a and E, * $P < 0.05$, ** $P < 0.01$, *** $P < 0.001$ vs. empty vector group. For F, G and I-R, * $P < 0.05$, ** $P < 0.01$, *** $P < 0.001$ vs. empty vector + siNC group; # $P < 0.05$, ## $P < 0.01$, ### $P < 0.001$ vs. NR3C1 Enhc. + siNC group.

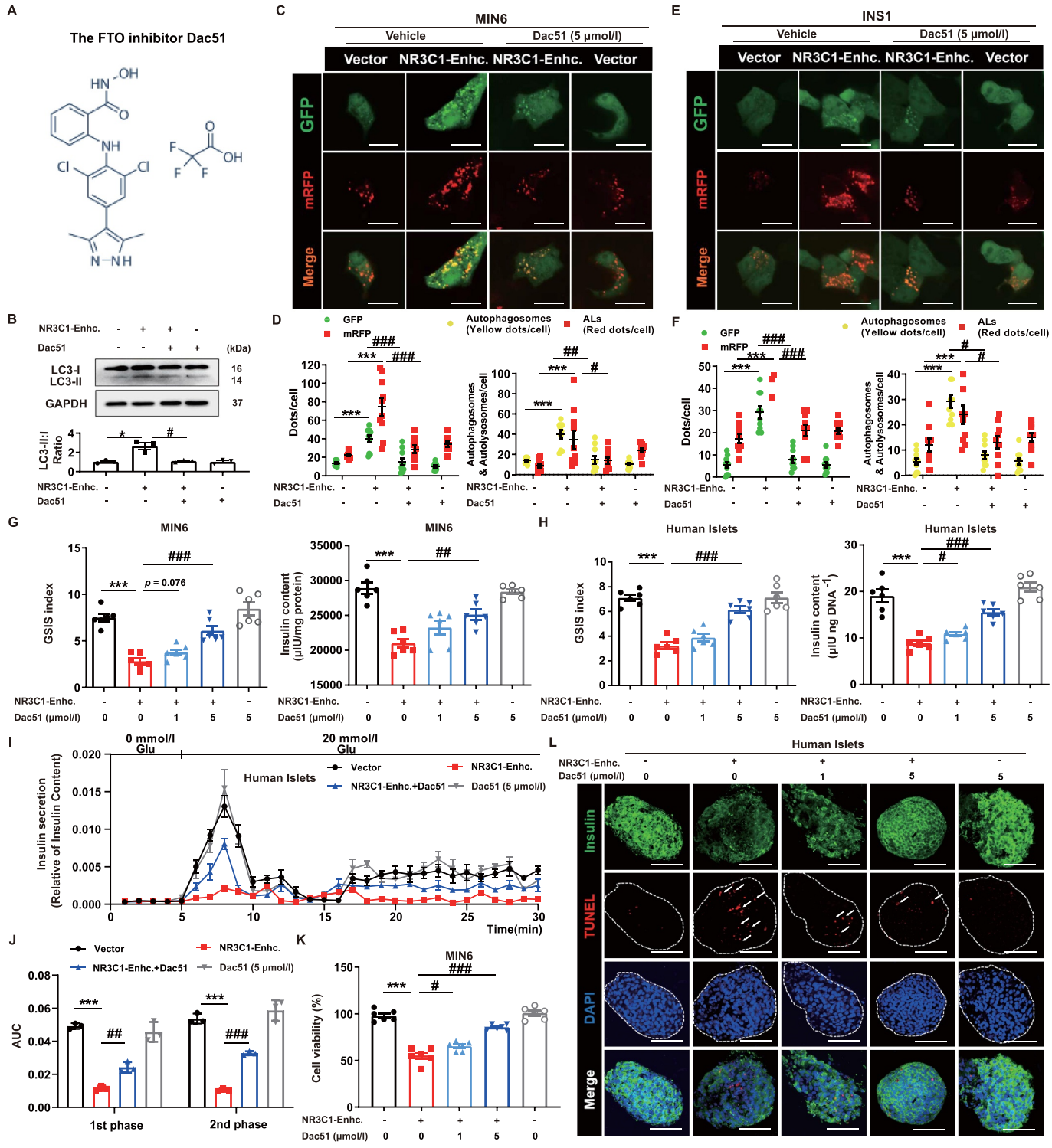

Figure 6. The FTO inhibitor Dac51 alleviates NR3C1-induced β-cell hyperactive autophagy and dysfunction. (A) Chemical structure of Dac51. (B) MIN6 cells were transfected with NR3C1-overexpressing plasmids or empty vectors and then treated with Dac51 (5 μmol/l) for 48 h. LC3 and SQSTM1 expression were measured by western blot. GAPDH was used as internal control. (C and D) MIN6 cells were transfected with Mrfp-GFP-LC3 adenovirus and the dots per cell were quantified in D ($n = 10$). Scale bar: 20 μm. (E and F) INS1 cells were transfected with Mrfp-GFP-LC3 and the dots per cell were quantified in F ($n = 10$). Scale bar: 20 μm. (G and H) GSIS analysis of control and NR3C1-overexpressing β-cells treated with or without Dac51. (I and J) Control and NR3C1-overexpressing human islets were treated with or without Dac51 for 48 h during islet perfusion in three separate experiments. AUC values for the 1st and 2nd phases of GSIS in islet perfusion were calculated in J. (K) Cell viability was evaluated in control and NR3C1-overexpressing MIN6 cell with or without Dac51 using CCK-8 assays. (L) TUNEL staining of cellular apoptosis of control and NR3C1-overexpressing human islets with or without Dac51 administration. The images of TUNEL positive cells were captured with a confocal laser. Data are presented as mean ± SEM. For B – K, * $P < 0.05$, ** $P < 0.01$, *** $P < 0.001$ vs. empty vector + vehicle group; # $P < 0.05$, ## $P < 0.01$, ### $P < 0.001$ vs. NR3C1-Enhc. + vehicle group.

Based on existed results, even though it is hard to distinguish the mechanisms between glucoxicity- or lipotoxicity-induced adaptive autophagy and glucolipotoxicity-induced deleterious autophagy, we determined that enhanced-NR3C1 was the key reason for "spoiled" autophagy in β-cells. For one thing, we did not observe NR3C1 upregulation in β-cells that

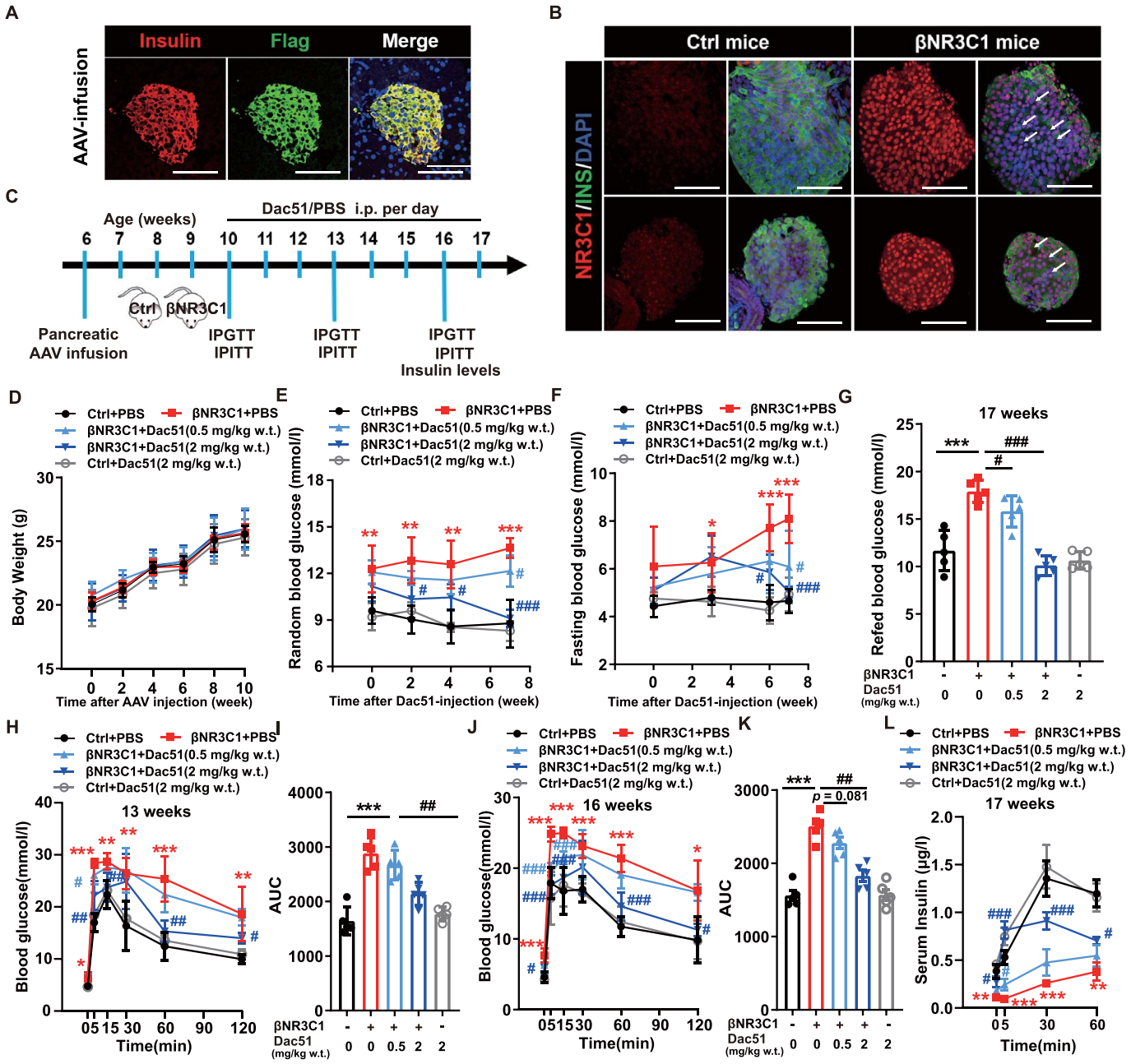

Figure 7. Dac51 improves glucose control and response in mice with β-cell-specific NR3C1 overexpression. (A and B) Male C57BL/6J mice (6 weeks old) were injected with AAV8-RIP2-vector or AAV8-RIP2-Nr3c1 via pancreatic intraductal viral infusion. AAV-vector expression (A) and NR3C1 enhancement (B) in pancreatic β-cells was confirmed via immunofluorescence. Scale bar: 100 μm. (C) 4 weeks after infusion, Ctrl and βNR3C1 mice were i.P. with PBS or Dac51 (2 or 0.5 mg/kg body weight) for 7 weeks. IPGTTs (intraperitoneal glucose tolerance tests), IPITTs (intraperitoneal insulin tolerance tests) and serum insulin levels were measured as indicated. (D) Body weight for mice in all 5 groups during Dac51 duration. (E) Random blood glucose levels were measured in mice from all groups for 7 weeks since Dac51 administration. (F) Fasting blood glucose levels were measured in mice from all groups for 7 weeks since Dac51 administration. (G) Refed blood glucose levels were measured in mice from all groups at 17 weeks. (H and I) IPGTTs were performed at 13 weeks. AUC were calculated in I. (J and K) IPGTTs were performed at 16 weeks. AUC were calculated in K. (L) Serum insulin levels after glucose stimulation were measured at 17 weeks by ELISA. Data are presented as mean ± SEM. For D – L, * $P < 0.05$, ** $P < 0.01$, *** $P < 0.001$ vs. Ctrl mice + PBS group; # $P < 0.05$, ## $P < 0.01$, ### $P < 0.001$ vs. βNR3C1 mice + PBS group.

exposed to purely prolonged glucose or palmitate; for another, NR3C1 did not participate in enhanced autophagy in the glucotoxicity or lipotoxicity-treated β-cells, indicated that NR3C1 plays a distinctive role in harmful excessive autophagy in glucolipotoxic conditions. NR3C1 controls many distinct gene networks in almost all cell types, including pancreatic β-cells. Unfortunately, there was a lack of systematic studies associated with molecular mechanisms for NR3C1 enhancement-induced β-cell failure before since only a few researchers have realized that excessive NR3C1 activity not only occurs in steroid diabetes but also plays vital roles in T2D pathogenesis [16,53,54]. Transcriptomics in our studies revealed that the top enriched pathways in NR3C1-overexpressed β-cells were linked primarily to autophagy, and we verified that NR3C1 conspicuously upregulated *Atg* genes expression, which orchestrates the process for

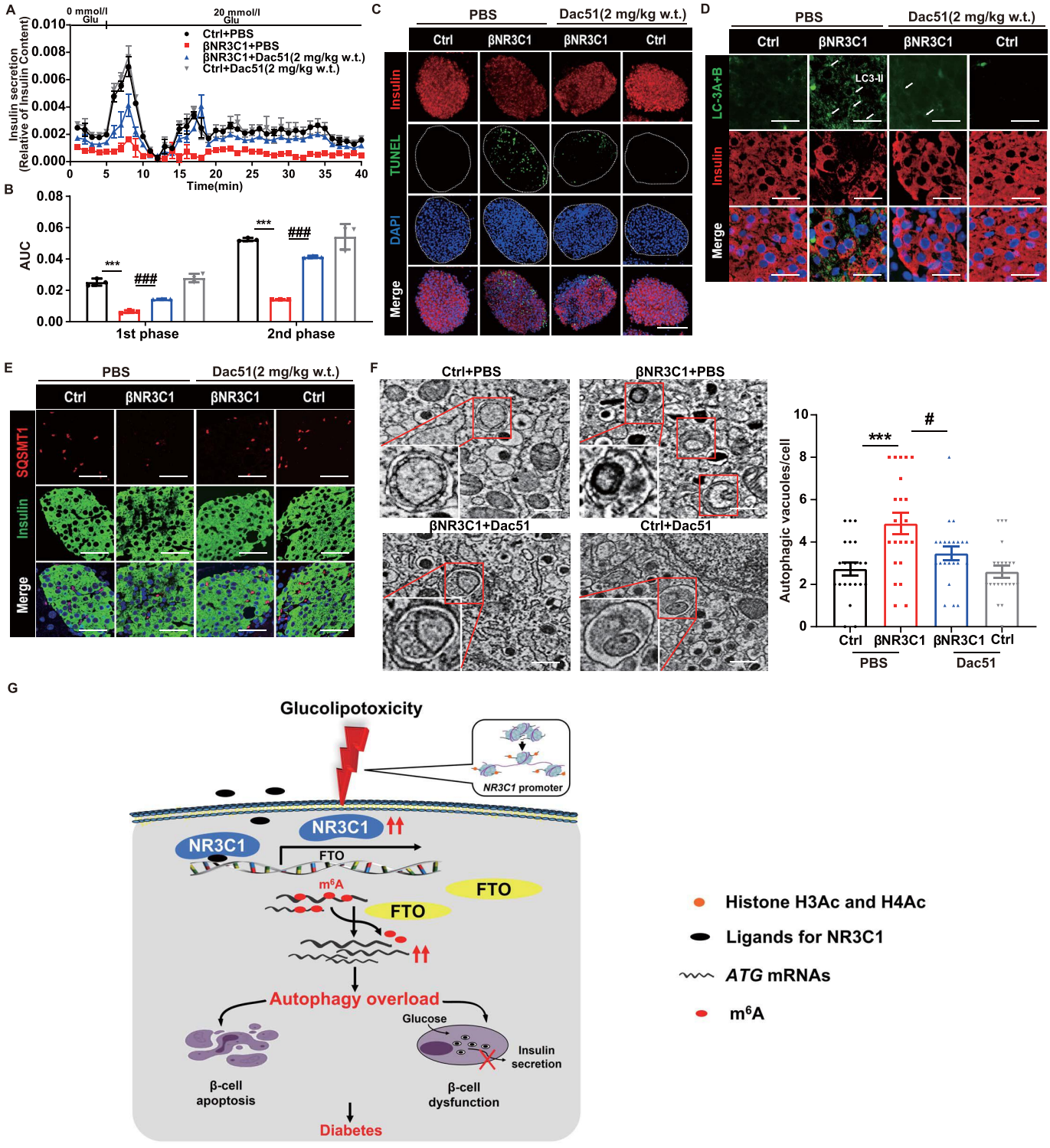

Figure 8. Dac51 reverses impaired insulin secretion and β-cell apoptosis by NR3C1-FTO-hyperactive autophagy axis in β-cells. (A and B) Islet perfusion was performed in βNR3C1 and Ctrl mice in three separate experiments. AUC values for the 1st and 2nd phases of GSIS in islet perfusion were calculated in B. (C) TUNEL staining of cellular apoptosis of islets in βNR3C1 and Ctrl mice. (D and E) Immunofluorescence staining of pancreatic sections obtained from βNR3C1 or Ctrl mice was performed for LC-3, SQSTM1, insulin, and DAPI. Scale bar: 100 μm. (F) Representative TEM images of pancreatic β-cells obtained from Ctrl mice and βNR3C1 mice. The number of autophagic structures was quantified in G ($n = 22$). Scale bar: 1 μm. Data are presented as mean ± SEM. For A, B and G, * $P < 0.05$, ** $P < 0.01$, *** $P < 0.001$ vs. Ctrl mice + PBS group; # $P < 0.05$, ## $P < 0.01$, ### $P < 0.001$ vs. βNR3C1 mice + PBS group. (G) Schematic representation of model. NR3C1 expression and activity is enhanced in pancreatic β-cells under glucolipotoxic status due to aberrantly increased H3Ac and H4Ac enrichment and chromatin accessibility at the NR3C1 Exon I_7 promoter. Upregulated NR3C1 transcriptional activity then activates RNA demethylase FTO, which diminishes m^6A modifications on autophagic transcripts (mainly Atg12, Atg5, Atg16l2 and Atg9a), ultimately promotes deleterious hyperactive autophagy and β-cell failure.

autophagy. Upregulated *Atg* gene levels are deeply involved in autophagy promotion [55,56], which was also reflected in NR3C1-stimulated β-cell autophagy.

Although it is widely accepted that gene activity can be affected by NR3C1 via direct and/or indirect DNA binding and regulation, recent studies have supplemented that NR3C1

also regulates RNA epigenetics, including m^{6}A modifications [57,58], which is consistent with our MeRIP-sequencing in that m^{6}A demethylation was crucial in NR3C1-induced harmful autophagy. Further studies revealed that NR3C1-induced RNA demethylase FTO expression played a major role in m^{6}A regulation that stabilized *Atg* gene expression. According to RNA-sequencing results, several *Atg* genes were upregulated upon NR3C1 overexpression, including *Atg10*, *Atg12*, *Atg5*, *Atg9a*, *Wipi1*, *Atg16l2* and *Pik3c3*. However, FTO deletion mainly reversed increased *Atg12*, *Atg5*, *Atg9a* and *Atg16l2* expression in NR3C1-overexpressing β-cells, which was parallel to retrieved autophagic flux, suggested that those four *Atg* genes act as core regulators in NR3C1-FTO-m^{6}A axis enhanced β-cell autophagy. In mammal cells, *Atg12*, *Atg5*, *Atg9a* and *Atg16l2* are included in the 20 core ATG proteins that strictly orchestrate autophagy [59]. Functionally, these 4 *Atg* gene products form different complexes (e.g., the ATG9A trafficking system and the ATG12–ATG5-ATG16L2 complex) that involved in the initiation and expansion steps of autophagosomes formation. In β-cells, ATG5 is critical not only in basal autophagy [60], but also in adaptive autophagy induced by stress [45,46]. Interestingly, some studies also demonstrate that ATG5 participates in the KISS1/kisspeptin or PDX1 deficiency-activated autophagy that suppresses basal insulin secretion and regulates β-cell-death [14,61], which is similar with our findings that ATG5 may exert deleterious effects on β-cell fate. ATG9a maintenances autophagosome formation to support mitochondrial activity and insulin secretion in β-cells [62], whether it plays roles in excessive autophagy has not been discussed. The roles of ATG12 and ATG16L2 are little known in β-cells, but upregulated ATG12 can enhance autophagy occurrence, for example, in breast cancer cells [63]. Since the protective autophagy in response to stress is still not fully elucidated in β-cells, our present work cannot tell the specific differences between the NR3C1-induced detrimental autophagy and the adaptive stress for now, but at least make it clear that the activity of these 4 *Atg*s may be appreciable features that distinguish the two.

According to our work, FTO is the key for abnormal *Atg*s. FTO has been found to play a key role in regulating transcriptome-wide m^{6}A modification in mRNA and is one of the m^{6}A regulators that has been associated with metabolic disorders such as diabetes and obesity [53]. In human, FTO is positively correlated with serum glucose. In T2D patients, lower m^{6}A levels are detected in mRNAs in blood, which is also related to higher FTO expression [53,64]. In pancreatic islets, functional characterizations of FTO in gene regulation warrants further dissection. In our studies, both ChIP and luciferase assays proved that FTO was activated by NR3C1 and acted as one component of NR3C1 signaling in the regulation of β-cell dysfunction. In fact, NR3C1-mediated transactivation of FTO and m^{6}A demethylation has also been indicated in the liver, which contributes to lipogenic gene activation in corticosterone or dexamethasone-induced lipid accumulation [57]. Using MeRIP-seq analysis, we firstly showed the descriptions of m^{6}A changes on *Atg* gene mRNAs in NR3C1-enhanced β-cell models *in vitro*. FTO-driven m-^{6}A modification directs mRNAs to distinct fates by grouping them for differential processing, translation, and degradation in the process, including autophagy regulation [65,66]. In our research, regarding *Atg12*, *Atg5*, *Atg9a* and *Atg16l2*, which were significantly involved in NR3C1-FTO axis-regulated β-cell autophagy, FTO mainly erased m^{6}A modifications in the 3'UTR regions of their mRNAs. We further demonstrated that FTO stabilized *Atg12*, *Atg5*, *Atg9a* and *Atg16l2* mRNA and mediated their activation upon NR3C1 overexpression, while it is still unclear whether YTHDF (YT521-B homology domain family) proteins that induce m^{6}A-containing RNAs deadenylation and degradation are also involved in NR3C1-FTO-mediated *Atg* genes expression [67]. Our studies indicated that FTO-m^{6}A modifications contribute to NR3C1-stimulated *Atg12*, *Atg5, Atg9a and Atg16l2* expressions, thereby triggering excessive autophagy activation and β-cell failure, which confirmed again that reduced RNA methylation in key β-cell genes was a significant contributor to the pathophysiology of β-cell dysfunction and diabetes.

It has been suggested that therapeutic targeting of m^{6}A regulators in a β-cell-specific manner in combination with current therapeutic agents might be a new avenue to counter declined m^{6}A levels in diabetic islets and to promote β-cell function and survival [68]. Based on this, we attempted to intervene the expression and/or activity of FTO to prevent NR3C1-induced β-cell failure and diabetes. The small molecule compound Dac51 is one newly developed FTO specific inhibitor that exerts more potent inhibitory activity on FTO demethylation activity, which has been reported to block FTO-mediated immune evasion and synergize with checkpoint blockade for better tumor control [44]. According to our observations, Dac51 protected against excessive autophagy activation, impaired insulin release and β-cells apoptosis resulted from NR3C1 enhancement both *ex vivo* and *in vitro*. To further evaluate the therapeutic effect of Dac51 *in vivo*, we forced NR3C1 expression via AAV-pancreatic viral infusion and generated βNR3C1 mice with an increased NR3C1 signaling only in β-cells. Metabolic phenotype analysis revealed that Dac51 administration for only 2–3 weeks could dose-dependently alleviate diabetic phenotypes manifested as hyperglycemia and impaired glucose tolerance in βNR3C1 mice, and with the prolonged medication time, blood glucose levels, glucose tolerance and serum insulin levels were further approaching the levels in control mice. All these observations reconfirmed the important regulatory role of the NR3C1-FTO axis in β-cell dysregulated autophagy and diabetes. Moreover, we also observed that there existed autophagy-independent harmful effect of FTO on β-cells, which was attributed to erroneous expression of genes related with reactive oxygen species accumulation, β-cell "key" genes and β-cell "disallowed" genes [69] (Figure S6). Collectively, our studies revealed that, adding to its anti-tumor properties, Dac51 also targeted to NR3C1-FTO axis to block β-cell failure and hyperglycemia, which further established its potential effectiveness in anti-diabetes.

Finally, our studies implied that NR3C1 upregulation is both necessary and sufficient to trigger insulin secretion disorders that further develop into various types of diabetes that featured β-cell failure. Although studies over the past two decades have indicated that NR3C1 mediates steroid

hormones excess-stimulated β-cell dysfunction which causes hyperglycemia and steroid-induced diabetes, NR3C1 also contributes to T2D β-cell failure [16,53,54], while little is known about the key mechanism. Our research demonstrated that NR3C1 expression, especially nuclear accumulation, was significantly elevated in T2D human islets, which mainly due to glucolipotoxic stress conditions. Those observations suggested that, even if clinical investigations have shown that some T2D subjects do have increased plasma steroid hormones levels [30,70], NR3C1 overactivation in T2D β-cells is also closely related to hyperglycemia and obesity status. Importantly, according to our m^{6}A methylome, NR3C1 overexpression resulted in dramatic declined m^{6}A levels accompanied with impaired insulin secretion in β-cells, which was consistent with the decreased m^{6}A levels in T2D islets as previously described [68]. Therefore, besides the autophagy overload discussed above, there might still be other potential molecular mechanisms underlying β-cell dysfunction induced by excessive NR3C1 that have not been fully studied here. Further work on this subject is remained to be continued in the future.

In summary, our observations indicated that NR3C1 is continuously enhanced in diabetic β-cells and associated with impaired insulin secretion and apoptosis, which mediated by NR3C1-FTO-m^{6}A modifications-*Atg* genes. Dac51 targeted FTO and protects against excessive autophagy-induced β-cell failure and impaired glucose metabolism in β-cell specific NR3C1-overexpressing models. These findings not only reveal the pathological importance of excessive NR3C1 in β-cell dysfunction and diabetes, but also establish the therapeutic importance of targeting FTO to prevent dysregulated autophagy and treat diabetes.

Materials and methods

Islet isolation and insulin secretion assay

Non-diabetic and T2D human islets were provided from Tianjin First Central Hospital. Islets isolation and culture, islets and β-cell line GSIS assay, and islets perfusion analysis were performed, as previously described [71]. The use of human primary islets was approved by the Research Ethics Committee of Nanjing Medical University and the research ethics committee of Tianjin First Central Hospital (ethics approval number: 2018N112KY).

Cell culture and high glucose and palmitate treatment

The mouse pancreatic β-cell lines MIN6 and rat pancreatic β-cell lines INS1 were cultured as described previously in medium supplemented with 15% or 8% FBS (Gibco, 10270–106) or charcoal-stripped FBS (i.e., steroids hormones-removed; Hyclone, SH30406.05), respectively [26]. Chronic high glucose and palmitate treatment was performed as previously described [72]. In brief, cells were cultured in a modified medium containing 0.5% (w:v) BSA (Best Biological Technology, MB4219–3), different concentrations of glucose (Sangon Biotech, A600219; low glucose: 5.5 mmol/l glucose +27.8 mmol/l mannitol for MIN6 cells, 5.5 mmol/l glucose +19.5 mmol/l mannitol for INS1 cells, and 5.5 mmol/l glucose+14.5 mmol/l mannitol for human islets; high glucose: 33.3 mmol/l for MIN6 cells and 25 mmol/l for INS1 for 48 h and 20 mmol/l for human islets for 48 h) and palmitate (0.2 mmol/l for INS-1 cells, 0.4 mmol/l for MIN6 cells and human islets). Mannitol (Sigma Aldrich, M4125) served as osmotic control.

NR3C1 agonists treatment

Cells or primary islets were cultured in a modified medium containing 0.5% (w:v) BSA, 200 nmol/l aldosterone (Sigma Aldrich, A9477) or 2 μmol/l dexamethasone (Sigma Aldrich, D4902) for 24–72 h according to the experimental requirement. Absolute ethanol served as solvent control.

Plasmid construction

pECMV-*Nr3c1-Flag*, pCMV-*Fto-Myc*, pGL3-basic-GRE-luciferase reporter (luc), pGL3-basic-*Fto*-luc, wild-type and mutant *Atg5*, *Atg12*, *Atg16l2*, *Atg9a*-3'UTR-luc were generated using a Mut Express MultiS Fast Mutagenesis Kit V2 (Vazyme Biotech, C215–01) according to the manufacturer's instructions.

Chromatin accessibility by real-time PCR assay (CHART-PCR)

Chromatin accessibility assays were performed as described previously [73,74]. In brief, MIN6 and INS-1 cells (5×10^6 cells/sample) were lysed by ice-cold Nonidet *P*-40 lysis buffer (10 mmol/l Tris-HCl, pH 7.4, 10 mmol/l NaCl, 3 mmol/l $MgCl_2$, 0.5% Nonidet *P*-40 (Diamond Biotechnology, 9016-45-9)), 0.15 mmol/l spermine (Sigma Aldrich, S4264), and 0.5 mmol/l spermidine (Sigma Aldrich, S0266) and incubated on ice for 10 min. Nuclei were isolated by centrifugation at 600 g for 5 min and washed with DNase I digestion buffer (50 mmol/l Tris-HCl, pH 8.0, 100 mmol/l NaCl, 3 mmol/l $MgCl_2$, 0.15 mmol/l spermine, 0.5 mmol/l spermidine) without $CaCl_2$. After centrifuge, nuclei were resuspended in DNase I digestion buffer supplemented with 1 mmol/l $CaCl_2$ (so called Buffer A) and incubated at 37°C for 1 min. Nuclease treatment was then achieved with DNase I (Takara, 2270A) with various concentrations, before which samples without DNase I addition were excluded from each group to monitor DNase I activity. Reactions were stopped by addition of 0.5 mol/l EDTA, Buffer A, 25 mg/ml proteinase K (Sigma Aldrich, P2308) and 20% SDS (w:v). Genomic DNA was isolated using a FastPure Cell/Tissue DNA Isolation Mini kit (Vazyme Biotech, DC102–01), and RT-qPCR was then performed to quantify target sequences. The primers are shown in Table S3. To correlate the Ct values (threshold values) from the amplification plots to percent accessibility, a standard curve was generated using serial dilutions of genomic DNA (0 ng, 0.8 ng, 4.0 ng, 20 ng, 100 ng, 500 ng), and chromatin accessibility was calculated and plotted as average percentages of the undigested sample among the total template genomic DNA.

Insulin biosynthesis

After overnight culture, islets were washed and then pulse-labeled in groups of 300–400 in 100 µl of medium containing 500 µCi each of [^{35}S]methionine (1,000 Ci µmmol) and (China Isotope & Radiation Corporation, 39556) at 37°C. Labeled islets were then rinsed, divided into batches, and incubated for chase periods up to 3 h in medium containing 20 mmol/l glucose and 20 µg/ml of unlabeled methionine. After the pulse and chase incubations, the newly synthesized insulin was analyzed as previously described [75,76].

RNA-sequencing and quantitative RT-PCR analysis

Cellular RNA of β-cell lines or islets were isolated using Trizol reagent (Takara, 9108). MIN6 total RNA were extracted, and a total amount of 3 µg RNA per sample was used as input material for the RNA sample preparations. Sequencing libraries were generated using NEBNext® UltraTM RNA Library Prep Kit for Illumina® (NEB, USA) following manufacturer's recommendations and index codes were added to attribute sequences to each sample. Clustering, sequencing and data analysis were done by Novogene Bioinformatics Technology (Tianjin, China). For qRT-PCR, cDNA was prepared from RNA using the SYBR Green PCR Master Mix (Vazyme Biotech, Q321–02), and quantitative RT-PCR was performed using a LightCycler480 II Sequence Detection System (Roche, Switzerland) as previously described [71]. Data were normalized by *Actb/actin*, and mRNA changes were calculated by the comparative ΔCt method. The primer sequences are shown in Table S5.

m^{6}A-RNA immunoprecipitation-sequencing (MeRIP-seq) and MeRIP-PCR

For MeRIP-seq, the mRNA m^{6}A was sequenced by MeRIP-seq at Novogene Bioinformatics Technology (Tianjin, China). Briefly, a total of 300 µg RNAs were extracted from MIN6 cells transfected with NR3C1-overexpressing plasmids or its empty vectors. The integrity and concentration of extracted RNAs were detected using an Agilent 2100 bioanalyzer (Agilent, USA) and simpliNano spectrophotometer (GE Healthcare, USA), respectively. Fragmented mRNA (~100 nt) was incubated for 2 h at 4°C with anti-m^{6}A polyclonal antibody (Cell Signaling technology, 56593S) in the immunoprecipitation experiment. Then, immunoprecipitated mRNAs or Input was used for library construction with NEBNext ultra RNA library prepare kit for Illumina (New England Biolabs, E7770). The library preparations were sequenced on an Illumina Novaseq or Hiseq platform with a paired-end read length of 150 bp according to the standard protocols. For MeRIP-PCR, total RNA was isolated from MIN6 cells and chemically fragmented to approximately 100 nt in size, ethanol-precipitated and separated on a 1.5% agarose gel. m^{6}A immunoprecipitation was performed as described previously [65]. m^{6}A+ RNA was purified using phenol/chloroform extraction and analyzed using RT-qPCR, and the primers for MeRIP are shown in Table S6.

mRNA stability analysis

Briefly, the cells were treated with 10 µg/ml actinomycin D (Sigma Aldrich, SBR00013) to inhibit global mRNA transcription. After incubation for the indicated time points, cells were collected and RNA samples were extracted for reverse transcription. The mRNA levels of interest were measured using qPCR [65].

Animal experiments

Male C57BL/6 aged five-six weeks were purchased from the Animal Core Facility of Nanjing Medical University. To establish a T2D model, the mice were housed in cages (5 per cage), reared under a 12-h light/12-h dark cycle with free access to water, and fed either with a normal diet consisting of standard lab chow or with a high-fat diet (HFD; Research Diets, D12492) containing 60% kcal from fat for 16–20 weeks until the mice in the HFD group showed a sustained elevated blood glucose level, an impaired glucose tolerance, and an insulin resistance. For pancreatic intraductal viral infusion assay, the mice were injected with adeno-associated virus serotype 8 vector (AAV8)-*RIP2* (Rat *Insulin-2* promoter)-*Nr3c1–3×Flag* (Hanbio Biosciences, HH20200702WY-AAV01) or with control virus (Hanbio Biosciences, HBAAV-1005). The viruses (10^{12} genome copy particle/ml) were infused at a rate of 6 µl/min by pancreatic intraductal viral infusion as described previously [77]. All animal experiments were conducted strictly following the guidelines and rules formulated by the Animal Care Committee of Nanjing Medical University.

Dac51 treatment

Dac51 treatment was freshly prepared by dissolving Dac51 (>99% purity; Selleck Chemicals, S9876) in dimethyl sulfoxide (DMSO) and then diluted with phosphate-buffered saline (PBS; Servicebio Technology, G4202). Dac51 was administrated via i.p. once daily (2 or 0.5 mg/kg body weight). Daily i.p. of an equivalent volume of PBS was given as the vehicle control.

Glucose and insulin tolerance tests

After a 16-h fast, the mice were i.p. with 2 g/kg body weight of glucose, and their blood glucose level was measured 0, 5, 15, 30, 60, and 120 min after injection. Blood samples were collected at all time points for plasma insulin measurements using ELISA test kits (EZassay Biotechnology, MS100). For insulin tolerance test, the mice were i.p. with 1 U/kg body weight of insulin after a 4-h fasting, and their blood glucose level was measured 0, 5, 15, 30, 60, 120 min after injection.

Immunofluorescence staining and image acquisition

Pancreases obtained from mice were fixed in 10% formalin and then embedded in paraffin for sectioning. The paraffinized sections were heated for 15 min at 55°C, deparaffinized (2 × 100% xylene for 5 min each, 2 × 100% ethanol for 5 min each, 2 × 95% ethanol for 5 min each, and 70% ethanol

for 5 min), and then rinsed in ddH_2O for 5 min. Antigen retrieval was performed by heating the slides at 100°C for 8 min in an acidic retrieval solution. The samples were blocked in 3% (w:v) BSA for 15 min at room temperature (RT) before incubating at 4°C overnight with the following primary antibodies diluted in 3% BSA: anti-NR3C1/GR (Cell Signalling Technology, 12041), anti-insulin (Servicebio Technology, GB12334), anti-LC3A/B (Cell Signaling Technology, 12741), anti-SQSTM1/p62 (Proteintech Group, 18420–1-AP) and anti-FTO (Invitrogen, 712913). After washing, the specimens were incubated in fluorochrome-conjugated secondary antibody diluted in 3% BSA for 1 h at RT in the dark. Nuclei were stained with DAPI (Sigma Aldrich, D9542) and then secured with a coverslip. Images were obtained using a laser scanning microscope (Olympus, Japan).

Western blot analysis

Pancreatic β-cells and isolated primary islets were lysed with ice-cold lysis buffer, and protein concentration in the cell lysate was quantified using the DC protein assay kit (Takara, T9300A). After protein content determination was conducted using a DC Protein Assay kit (Bio-Rad Laboratories, 500–0111), and western blot analysis was performed, as described previously [78].

Cell counting Kit-8 (CCK-8) assay

Cells were seeded in 48-well plates (4×10^4 cells/well) in 200 µl culture medium. CCK-8 assay was performed according to the manufacturer's protocol (Vazyme Biotech, A311–01/02).

TUNEL staining

The suspension cultures of treated islet cells were fixed for 0.5 h. Terminal dUTP nick-end labeling (TUNEL) was performed using a commercially available kit (Vazyme Biotech, A113–01) and specifically according to the manufacturer's protocol. TUNEL imaging and quantitation of human islet sections and MIN6 cells were observed under laser scanning confocal microscope (Olympus, Japan).

Flow cytometry assay

MIN6 cells were grown in the wells of 6-well plates and harvested by trypsinization. Following double staining with FITC-ANXA5/annexin V and propidium iodide (PI) (Vazyme Biotech, A211–01/02), the cells were analyzed using flow cytometry (BD Biosciences, USA).

Autophagy detection using Mrfp-GFP-LC3 adenoviral vector

Autophagic flux was measured by transfecting tandem mRFP-GFP-LC3 recombinant adenovirus (Hanbio Biosciences, HB-AP210 0001). MIN6 cells were plated in a 6-well plate and allowed to reach 50%–70% confluence at the time of transfection. Adenoviral infection was performed according to the manufacturer's instructions. Autophagy was observed under a laser scanning confocal microscope (Olympus, Japan). Autophagic flux was determined by evaluating the number of GFP and mRFP puncta (puncta/cell were counted). Yellow (merge of GFP signal and RFP signal) puncta represented early autophagosomes, while red (RFP signal alone) puncta indicate late autolysosomes.

Transmission electron microscopy (TEM)

Islets extracted from mice were fixed with 2.5% glutaraldehyde in 0.1 mol/l sodium cacodylate buffer for 2 h and then post-fixed in 1% OsO_4, 1.5% $K_4Fe(CN)_6$, and 0.1 mol/L sodium cacodylate for 1 h. Islets were en bloc stained, dehydrated, embedded, and cut into ultrathin sections (50–80 nm). The samples were visualized using a Tecnai Spirit Biotwin operated at 200 kV (FEI Company, USA).

Chromatin immunoprecipitation (ChIP) assay

At least 2×10^7 cells were used for each experiment. Chromatin was crosslinked with 1% formaldehyde for 10 min at RT, and cross-linking was terminated using 0.125 mol/l glycine. Cells were collected after two washings with iced PBS in a lysis buffer (1% SDS, 10 mmol/l EDTA, 50 mmol/l Tris-HCl, pH 8.1, 1 mmol/l phenylmethylsulfonyl fluoride (Sangon Biotech, A610425), 2×10^6 cells/200 µl) and then sonicated on ice. After centrifugation, 20 µl of the supernatants were used as inputs, and the remaining portion was diluted five-fold with ChIP dilution buffer (0.01% SDS, 1.1% Triton X-100 (Sangon Biotech, A600198), 1.2 mmol/l EDTA, 16.7 mmol/l Tris-HCl, pH 8.1, 167 mmol/l NaCl, 1 mmol/l phenylmethylsulfonyl fluoride). The diluted fraction was subjected to immunoprecipitation overnight after 1 h of preclearing at 4°C with 30 µl salmon sperm DNA/protein A beads (Millipore, 16–157). Complexes were recovered through a 2–4 h incubation at 4°C with 60 µl salmon sperm DNA/protein A beads. Precipitates were serially washed with 1 ml low salt immune complex wash buffer (0.1% SDS, 1% Triton X-100, 2 mmol/l EDTA, 20 mmol/l Tris-HCl, pH 8.1, 150 mmol/l NaCl), high salt immune complex wash buffer (0.1% SDS, 1% Triton X-100, 2 mmol/l EDTA, 20 mmol/l Tris-HCl, pH 8.1, 0.5 mol/l NaCl), LiCl immune complex wash buffer (LiCl 0.25 mol/l, 1% NP-40, 0.1 mmol/l EDTA, 24.1 mmol/l $C_{24}H_{39}O_4Na$ (Sangon Biotech, A600150), 10 mmol/l Tris-HCl, pH 8.1) and twice with TE buffer (1 mmol/l EDTA, 10 mmol/l Tris-HCl, pH 8.1). Precipitated chromatin complexes were removed from the beads through a 15-min incubation with 100 µl ChIP elution buffer (2.9% SDS, 28.6 mmol/l $NaHCO_3$), and this procedure was repeated. DNA was extracted and purified and then subjected to PCR using designed primers. The primers for ChIP are shown in Table S3. All the buffers mentioned above contained protease inhibitor cocktail (Roche, 04693124001).

Transient transfection and dual-luciferase reporter assay

Transient transfection with plasmids and small interfering RNA (siRNA) was performed with Lipofectamine 2000 (Mei5 Biotechnology, MF135–02), as previously described [71]. Adenovirus-NR3C1/GR and its control virus were purchased from Genechem (GOSA0321320). Specific siRNA for *Nr3c1* (si*Nr3c1*) and *Fto* (si*Fto*) was purchased from GenePharma (A01001). The siRNA sequences are shown in Table S4. The luciferase activity was assessed using the reporter constructs and the Dual-Glo Luciferase Assay System (Vazyme Biotech, DL101–01) on a TD-20/20 Luminometer (Turner BioSystems, USA).

Statistical analysis

All experiments were performed at least in biological triplicate. Comparisons were performed using Student's t-test for two groups. Data are presented as mean ± SEM. *P* values of less than 0.05 were considered statistically significant and are provided in the figures.

Acknowledgements

This work was supported by the National Natural Science Foundation of China (81830024 to X.H., 81970673 to F.C., 82000738 to T-J.W.) and the Natural Science Foundation of Jiangsu Province (BK20200670 to T-J.W.). This work was also supported by the Natural Science Research of Jiangsu Higher Education Institutions of China (20KJB310001 to T-J.W.). X.H. and F.C. are the guarantors of this work and, as such, had full access to all the data in the study and take responsibility for the integrity of the data and the accuracy of the data analysis.

Disclosure statement

The authors disclose no financial conflict of interest.

Funding

The work was supported by the National Natural Science Foundation of China [81830024]; National Natural Science Foundation of China [81970673]; National Natural Science Foundation of China [82000738]; Natural Science Foundation of Jiangsu Province [BK20200670]; Natural Science Research of Jiangsu Higher Education Institutions of China [20KJB310001]

Data availability statement

All relevant datasets generated during and/or analyzed during the current study are available from the corresponding authors upon reasonable request. RNAseq data that support the findings of this study have been deposited in the NCBI's Gene Expression Omnibus (GEO) under accession code GSE182267 (https://www.ncbi.nlm.nih.gov/geo/query/acc.cgi?acc=GSE182267). MeRIPseq data that support the findings of this study have been deposited in the GEO under accession code GSE182268 (https://www.ncbi.nlm.nih.gov/geo/query/acc.cgi?acc=GSE182268).

ORCID

Tijun Wu http://orcid.org/0000-0002-8788-5686
Xiao Han http://orcid.org/0000-0002-6467-1802

References

[1] Bagnati M, Ogunkolade BW, Marshall C, et al. Glucolipotoxicity initiates pancreatic beta-cell death through TNFR5/CD40-mediated STAT1 and NF-kappaB activation. Cell Death Dis. 2016;7(8):e2329. DOI:10.1038/cddis.2016.203
[2] Lee YH, Kim J, Park K. Lee MS: beta-cell autophagy: mechanism and role in beta-cell dysfunction. Mol Metab. 2019;27S:S92–103.
[3] Weir GC, Marselli L, Marchetti P, et al. Towards better understanding of the contributions of overwork and glucotoxicity to the beta-cell inadequacy of type 2 diabetes. Diab Obes Metab. 2009;11(Suppl 4):82–90.
[4] Mizushima N, Komatsu M. Autophagy: renovation of cells and tissues. Cell. 2011;147(4):728–741.
[5] Levine B, Kroemer G. Biological functions of autophagy genes: a disease perspective. Cell. 2019;176(1–2):11–42.
[6] Mazza S, Maffucci T. Autophagy and pancreatic beta-cells. Vitam Horm. 2014;95:145–164.
[7] Xing QC, Liu X, Li W, et al. Sangguayin preparation prevents palmitate-induced apoptosis by suppressing endoplasmic reticulum stress and autophagy in db/db mice and MIN6 pancreatic beta-cells. Chin J Nat Med. 2020;18(6):472–480.
[8] Wang J, Li D, Zhang Z, et al. Autoantibody against angiotensin II type I receptor induces pancreatic beta-cell apoptosis via enhancing autophagy. Acta Biochim Biophys Sin (Shanghai). 2021;53(6):784–795.
[9] Sramek J, Nemcova-Furstova V, Kovar J. Molecular mechanisms of apoptosis induction and its regulation by fatty acids in pancreatic β-cells. Int J Mol Sci. 2021;22(8):4285.
[10] Darwish MA, Abdel-Bakky MS, Messiha BAS, et al. Resveratrol mitigates pancreatic TF activation and autophagy-mediated beta cell death via inhibition of CXCL16/ox-LDL pathway: a novel protective mechanism against type 1 diabetes mellitus in mice. Eur J Pharmacol. 2021;901:174059.
[11] Chen ZF, Li YB, Han JY, et al. The double-edged effect of autophagy in pancreatic beta cells and diabetes. Autophagy. 2011;7(1):12–16.
[12] Masini M, Bugliani M, Lupi R, et al. Autophagy in human type 2 diabetes pancreatic beta cells. Diabetologia. 2009;52(6):1083–1086.
[13] Ahlgren U, Jonsson J, Jonsson L, et al. Beta-cell-specific inactivation of the mouse Ipf1/Pdx1 gene results in loss of the beta-cell phenotype and maturity onset diabetes. Genes Dev. 1998;12(12):1763–1768.
[14] Fujimoto K, Hanson PT, Tran H, et al. Autophagy regulates pancreatic beta cell death in response to Pdx1 deficiency and nutrient deprivation. J Biol Chem. 2009;284(40):27664–27673.
[15] Tanemura M, Ohmura Y, Deguchi T, et al. Rapamycin causes upregulation of autophagy and impairs islets function both in vitro and in vivo. Am J Transplant. 2012;12(1):102–114. DOI:10.1111/j.1600-6143.2011.03771.x
[16] Aylward A, Okino ML, Benaglio P, et al. Glucocorticoid signaling in pancreatic islets modulates gene regulatory programs and genetic risk of type 2 diabetes. PLoS Genet. 2021;17(5):e1009531.
[17] Hoes JN, van der Goes MC, van Raalte DH, et al. Glucose tolerance, insulin sensitivity and beta-cell function in patients with rheumatoid arthritis treated with or without low-to-medium dose glucocorticoids. Ann Rheum Dis. 2011;70(11):1887–1894. DOI:10.1136/ard.2011.151464
[18] Di Dalmazi G, Pagotto U, Pasquali R, et al. Glucocorticoids and type 2 diabetes: from physiology to pathology. J Nutr Metab. 2012;2012:525093.
[19] Delaunay F, Khan A, Cintra A, et al. Pancreatic beta cells are important targets for the diabetogenic effects of glucocorticoids. J Clin Invest. 1997;100(8):2094–2098.
[20] Hwang JL, Weiss RE. Steroid-induced diabetes: a clinical and molecular approach to understanding and treatment. Diabetes Metab Res Rev. 2014;30(2):96–102.
[21] Schacke H, Docke WD, Asadullah K. Mechanisms involved in the side effects of glucocorticoids. Pharmacol Ther. 2002;96(1):23–43.
[22] Esguerra JLS, Ofori JK, Nagao M, et al. Glucocorticoid induces human beta cell dysfunction by involving riborepressor GAS5 LincRNA. Mol Metab. 2020;32:160–167.

[23] Colvin ES, Ma HY, Chen YC, et al. Glucocorticoid-induced suppression of beta-cell proliferation is mediated by Mig6. Endocrinology. 2013;154(3):1039–1046.
[24] Sato S, Saisho Y, Inaishi J, et al. Effects of glucocorticoid treatment on beta- and alpha-cell mass in Japanese adults with and without diabetes. Diabetes. 2015;64(8):2915–2927.
[25] Kaiser G, Gerst F, Michael D, et al. Regulation of forkhead box O1 (FOXO1) by protein kinase B and glucocorticoids: different mechanisms of induction of beta cell death in vitro. Diabetologia. 2013;56(7):1587–1595.
[26] Chen F, Liu J, Wang Y, et al. Aldosterone induces clonal beta-cell failure through glucocorticoid receptor. Sci Rep. 2015;5:13215.
[27] Luther JM, Luo P, Kreger MT, et al. Aldosterone decreases glucose-stimulated insulin secretion in vivo in mice and in murine islets. Diabetologia. 2011;54(8):2152–2163.
[28] Luther JM, Brown NJ. The renin-angiotensin-aldosterone system and glucose homeostasis. Trends Pharmacol Sci. 2011;32(12):734–739.
[29] Sowers JR, Whaley-Connell A, Epstein M. Narrative review: the emerging clinical implications of the role of aldosterone in the metabolic syndrome and resistant hypertension. Ann Intern Med. 2009;150(11):776–783.
[30] Hollenberg NK, Stevanovic R, Agarwal A, et al. Plasma aldosterone concentration in the patient with diabetes mellitus. Kidney Int. 2004;65(4):1435–1439.
[31] Davani B, Portwood N, Bryzgalova G, et al. Aged transgenic mice with increased glucocorticoid sensitivity in pancreatic beta-cells develop diabetes. Diabetes. 2004;53(Suppl 1):S51–59.
[32] Blondeau B, Sahly I, Massourides E, et al. Novel transgenic mice for inducible gene overexpression in pancreatic cells define glucocorticoid receptor-mediated regulations of beta cells. PLoS ONE. 2012;7(2):e30210.
[33] Meduri GU, Annane D, Confalonieri M, et al. Pharmacological principles guiding prolonged glucocorticoid treatment in ARDS. Intensive care Med. 2020;46(12):2284–2296.
[34] Seo MK, Kim SG, Seog DH, et al. Effects of early life stress on epigenetic changes of the glucocorticoid receptor 17 promoter during adulthood. Int J Mol Sci. 2020;21(17):6331.
[35] Park SW, Lee JG, Seo MK, et al. Epigenetic modification of glucocorticoid receptor promoter I7 in maternally separated and restraint-stressed rats. Neurosci Lett. 2017;650:38–44.
[36] Fine NHF, Doig CL, Elhassan YS, et al. Glucocorticoids reprogram beta-cell signaling to preserve insulin secretion. Diabetes. 2018;67(2):278–290. DOI:10.2337/db16-1356
[37] Gesina E, Tronche F, Herrera P, et al. Dissecting the role of glucocorticoids on pancreas development. Diabetes. 2004;53(9):2322–2329.
[38] Liu X, Turban S, Carter RN, et al. Beta-cell-specific glucocorticoid reactivation attenuates inflammatory beta-cell destruction. Front Endocrinol. 2014;5:165.
[39] Ullrich S, Berchtold S, Ranta F, et al. Serum- and glucocorticoid-inducible kinase 1 (SGK1) mediates glucocorticoid-induced inhibition of insulin secretion. Diabetes. 2005;54(4):1090–1099. DOI:10.2337/diabetes.54.4.1090
[40] Jia G, Fu Y, Zhao X, et al. N6-methyladenosine in nuclear RNA is a major substrate of the obesity-associated FTO. Nat Chem Biol. 2011;7(12):885–887. DOI:10.1038/nchembio.687
[41] Zhao X, Yang Y, Sun BF, et al. FTO-dependent demethylation of N6-methyladenosine regulates mRNA splicing and is required for adipogenesis. Cell Res. 2014;24(12):1403–1419. DOI:10.1038/cr.2014.151
[42] Wang X, Lu Z, Gomez A, et al. N6-methyladenosine-dependent regulation of messenger RNA stability. Nature. 2014;505(7481):117–120. DOI:10.1038/nature12730
[43] Wang X, Zhao BS, Roundtree IA, et al. N(6)-methyladenosine modulates messenger RNA translation efficiency. Cell. 2015;161(6):1388–1399.
[44] Liu Y, Liang G, Xu H, et al. Tumors exploit FTO-mediated regulation of glycolytic metabolism to evade immune surveillance. Cell Metab. 2021;33(6):1221–1233 e1211. DOI:10.1016/j.cmet.2021.04.001
[45] Ebato C, Uchida T, Arakawa M, et al. Autophagy is important in islet homeostasis and compensatory increase of beta cell mass in response to high-fat diet. Cell Metab. 2008;8(4):325–332. DOI:10.1016/j.cmet.2008.08.009
[46] Bartolome A, Guillen C, Benito M. Autophagy plays a protective role in endoplasmic reticulum stress-mediated pancreatic beta cell death. Autophagy. 2012;8(12):1757–1768.
[47] Melmed RN, Benitez CJ, Holt SJ. Intermediate cells of the pancreas. 3. Selective autophagy and destruction of beta-granules in intermediate cells of the rat pancreas induced by alloxan and streptozotocin. J Cell Sci. 1973;13(1):297–315.
[48] Choi SE, Lee SM, Lee YJ, et al. Protective role of autophagy in palmitate-induced INS-1 beta-cell death. Endocrinology. 2009;150(1):126–134.
[49] Han D, Yang B, Olson LK, et al. Activation of autophagy through modulation of 5'-AMP-activated protein kinase protects pancreatic beta-cells from high glucose. Biochem J. 2010;425(3):541–551.
[50] Meijer AJ, Codogno P. Macroautophagy: protector in the diabetes drama? Autophagy. 2007;3(5):523–526.
[51] Poitout V, Amyot J, Semache M, et al. Glucolipotoxicity of the pancreatic beta cell. Biochim Biophys Acta. 2010;1801(3):289–298.
[52] Poitout V, Robertson RP. Glucolipotoxicity: fuel excess and beta-cell dysfunction. Endocr Rev. 2008;29(3):351–366.
[53] Shen F, Huang W, Huang JT, et al. Decreased N(6)-methyladenosine in peripheral blood RNA from diabetic patients is associated with FTO expression rather than ALKBH5. J Clin Endocrinol Metab. 2015;100(1):E148–154. DOI:10.1210/jc.2014-1893
[54] Koizumi M, Yada T. Sub-chronic stimulation of glucocorticoid receptor impairs and mineralocorticoid receptor protects cytosolic Ca^{2+} responses to glucose in pancreatic beta-cells. J Endocrinol. 2008;197(2):221–229.
[55] Rusmini P, Cortese K, Crippa V, et al. Trehalose induces autophagy via lysosomal-mediated TFEB activation in models of motoneuron degeneration. Autophagy. 2019;15(4):631–651. DOI:10.1080/15548627.2018.1535292
[56] Wang P, Nolan TM, Yin Y, et al. Identification of transcription factors that regulate ATG8 expression and autophagy in Arabidopsis. Autophagy. 2020;16(1):123–139.
[57] Hu Y, Feng Y, Zhang L, et al. GR-mediated FTO transactivation induces lipid accumulation in hepatocytes via demethylation of m(6)A on lipogenic mRnas. RNA Biol. 2020;17(7):930–942.
[58] Bartlett AA, Lapp HE, Hunter RG. Epigenetic Mechanisms of the Glucocorticoid Receptor. Trends Endocrinol Metab. 2019;30(11):807–818.
[59] Li X, He S, Ma B. Autophagy and autophagy-related proteins in cancer. Mol Cancer. 2020;19(1):12.
[60] Kim C, Kim W, Lee H, et al. The RNA-binding protein HuD regulates autophagosome formation in pancreatic beta cells by promoting autophagy-related gene 5 expression. J Biol Chem. 2014;289(1):112–121. DOI:10.1074/jbc.M113.474700
[61] Huang C, Wang HY, Wang ME, et al. Kisspeptin-activated autophagy independently suppresses non-glucose-stimulated insulin secretion from pancreatic beta-cells. Sci Rep. 2019;9(1):17451.
[62] Aoyagi K, Itakura M, Fukutomi T, et al. VAMP7 regulates autophagosome formation by supporting Atg9a functions in pancreatic beta-cells from male mice. Endocrinology. 2018;159(11):3674–3688.
[63] Zhang S, Liu X, Abdulmomen Ali Mohammed S, et al. Adaptor SH3BGRL drives autophagy-mediated chemoresistance through promoting PIK3C3 translation and ATG12 stability in breast cancers. Autophagy. 2021;18(8):1–19. DOI:10.1080/15548627.2021.2002108
[64] Yang Y, Shen F, Huang W, et al. Glucose is involved in the dynamic regulation of m6A in patients with type 2 diabetes. J Clin Endocrinol Metab. 2019;104(3):665–673.
[65] Wang X, Wu R, Liu Y, et al. M(6)a mRNA methylation controls autophagy and adipogenesis by targeting Atg5 and Atg7. Autophagy. 2020;16(7):1221–1235.
[66] Jin S, Zhang X, Miao Y, et al. M(6)a RNA modification controls autophagy through upregulating ULK1 protein abundance. Cell Res. 2018;28(9):955–957. DOI:10.1038/s41422-018-0069-8

[67] Du H, Zhao Y, He J, et al. YTHDF2 destabilizes m(6)A-containing RNA through direct recruitment of the CCR4-NOT deadenylase complex. Nat Commun. 2016;7:12626.
[68] De Jesus DF, Zhang Z, Kahraman S, et al. M(6)a mRNA methylation regulates human beta-cell biology in physiological states and in type 2 diabetes. Nat Metab. 2019;1(8):765–774.
[69] Lemaire K, Thorrez L, Schuit F. Disallowed and allowed gene expression: two faces of mature islet beta cells. Annu Rev Nutr. 2016;36:45–71.
[70] Hofmann A, Peitzsch M, Brunssen C, et al. Elevated steroid hormone production in the db/db mouse model of obesity and type 2 diabetes. Horm Metab Res. 2017;49(1):43–49. DOI:10.1055/s-0042-116157
[71] Wu T, Zhang S, Xu J, et al. HRD1, an important player in pancreatic beta-cell failure and therapeutic target for type 2 diabetic mice. Diabetes. 2020;69(5):940–953.
[72] Huang Q, You W, Li Y, et al. Glucolipotoxicity-inhibited mir-299-5p regulates pancreatic beta-cell function and survival. Diabetes. 2018;67(11):2280–2292.
[73] Gao L, Wu K, Liu Z, et al. Chromatin accessibility landscape in human early embryos and its association with evolution. Cell. 2018;173(1):248–259 e215. DOI:10.1016/j.cell.2018.02.028
[74] Lee CG, Kwon HK, Sahoo A, et al. Interaction of Ets-1 with HDAC1 represses IL-10 expression in Th1 cells. J Immunol. 2012;188(5):2244–2253. DOI:10.4049/jimmunol.1101614
[75] Zhu X, Orci L, Carroll R, et al. Severe block in processing of proinsulin to insulin accompanied by elevation of des-64,65 proinsulin intermediates in islets of mice lacking prohormone convertase 1/3. Proc Natl Acad Sci U S A. 2002;99(16):10299–10304.
[76] Furukawa H, Carroll RJ, Swift HH, et al. Long-term elevation of free fatty acids leads to delayed processing of proinsulin and prohormone convertases 2 and 3 in the pancreatic beta-cell line MIN6. Diabetes. 1999;48(7):1395–1401.
[77] Xiao X, Guo P, Prasadan K, et al. Pancreatic cell tracing, lineage tagging and targeted genetic manipulations in multiple cell types using pancreatic ductal infusion of adeno-associated viral vectors and/or cell-tagging dyes. Nat Protoc. 2014;9(12):2719–2724. DOI:10.1038/nprot.2014.183
[78] Chen F, Sha M, Wang Y, et al. Transcription factor Ets-1 links glucotoxicity to pancreatic beta cell dysfunction through inhibiting PDX-1 expression in rodent models. Diabetologia. 2016;59(2):316–324. DOI:10.1007/s00125-015-3805-3